International Journal of Earth Sciences (2018) 107:2465–2489
https://doi.org/10.1007/s00531-018-1608-8

ORIGINAL PAPER

A new U–Pb zircon age and a volcanogenic model for the early Permian Chemnitz Fossil Forest

Ludwig Luthardt[1,2] · Mandy Hofmann[3] · Ulf Linnemann[3] · Axel Gerdes[4] · Linda Marko[4] · Ronny Rößler[1,2]

Received: 3 November 2017 / Accepted: 28 March 2018 / Published online: 6 April 2018

Abstract

The Chemnitz Fossil Forest depicts one of the most completely preserved forest ecosystems in late Paleozoic Northern Hemisphere of tropical Pangaea. Fossil biota was preserved as a T^0 taphocoenosis resulting from the instantaneous entombment by volcanic ashes of the Zeisigwald Tuff. The eruption depicts one of the late magmatic events of post-variscan rhyolitic volcanism in Central Europe. This study represents a multi-method evaluation of the pyroclastic ejecta encompassing sedimentological and (isotope) geochemical approaches to shed light on magmatic and volcanic processes, and their role in preserving the fossil assemblage. The Zeisigwald Tuff pyroclastics (ZTP) reveal a radiometric age of 291 ± 2 Ma, pointing to a late Sakmarian/early Artinskian (early Permian) stratigraphic position for the Chemnitz Fossil Forest. The initial eruption was of phreatomagmatic style producing deposits of cool, wet ashes, which deposited from pyroclastic fall out and density currents. Culmination of the eruption is reflected by massive hot and dry ignimbrites. Whole-rock geochemistry and zircon grain analysis show that pyroclastic deposits originated from a felsic, highly specialised magma, which underwent advanced fractionation, and is probably related to post-Carboniferous magmatism in the Western Erzgebirge. The ascending magma recycled old cadomic crust of the Saxo-thuringian zone, likely induced by a mantle-derived heat flow during a phase of post-variscan crustal delamination. Geochemical trends within the succession of the basal pyroclastic horizons reflect inverse zonation of the magma chamber and provide evidence for the continuous eruption and thus a simultaneous burial of the diverse ecosystem.

Keywords T^0 assemblage · Early Permian · Rhyolitic volcanism · Phreatomagmatic eruption · U–Pb zircon age · Hf isotopes

Introduction

Volcanically preserved fossil assemblages provide some of the most detailed insights into ancient biotas contributing to our understanding of complex geological and

Electronic supplementary material The online version of this article (https://doi.org/10.1007/s00531-018-1608-8) contains supplementary material, which is available to authorized users.

✉ Ludwig Luthardt
luthardt@mailserver.tu-freiberg.de

Mandy Hofmann
mandy.hofmann@senckenberg.de

Ulf Linnemann
ulf.linnemann@senckenberg.de

Axel Gerdes
gerdes@em.uni-frankfurt.de

Linda Marko
marko@em.uni-frankfurt.de

Ronny Rößler
roessler@naturkunde-chemnitz.de

[1] Museum für Naturkunde Chemnitz, Moritzstraße 20, 09111 Chemnitz, Germany

[2] Geologisches Institut, Technische Universität Bergakademie Freiberg, Bernhard-von-Cotta-Straße 2, 09599 Freiberg, Germany

[3] Senckenberg Naturhistorische Sammlungen Dresden, Museum für Mineralogie und Geologie, Sektion Geochronologie, Königsbrücker Landstraße 159, 01109 Dresden, Germany

[4] Institut für Geowissenschaften, Mineralogie, Goethe-Universität Frankfurt, Altenhöferallee 1, 60438 Frankfurt am Main, Germany

palaeoecological interrelations in past ecosystems, their change and concomitant biotic and abiotic responses, even far back in time (Spicer 1989; Schneider 1994; Scott et al. 1994; Rößler and Barthel 1998; Hilton et al. 2004; Kerp et al. 2007; Wang et al. 2012; Opluštil et al. 2014). A remarkable fossil forest is known from Chemnitz, Germany, where an early Permian landscape was buried instantaneously by volcanic deposits, preserving an autochthonous to parautochthonous fossil assemblage. Collecting and research at this site date back to the early 18th century and were continuously more or less in research focus since that time. Important finds were made in the late 19th and the early 20th centuries when outstanding anatomically preserved specimens provided the basis for the introduction of fossil plant names (Cotta 1832). Since 2008, a new quality in investigating the fossil forest was achieved, based on two scientific excavations in the urban area of Chemnitz. The first excavation in Chemnitz–Hilbersdorf (2008–2011) provided more than 2,000 finds of petrifactions, moulds, casts, and adpressions from different volcano-sedimentary units (Kretzschmar et al. 2008; Rößler et al. 2008, 2009, 2010, 2012a). Discoveries have so far yielded significant results on ancient plants, animals, palaeoecological interactions, and palaeoclimatic conditions (Dunlop and Rößler 2013; Feng et al. 2014; Dunlop et al. 2016; Luthardt et al. 2016, 2017; Spindler et al. 2018). Tree trunk bases still standing upright in their places of growth and rooting in the underlying palaeosol characterise this fossil lagerstätte as a significant T^0 assemblage sensu DiMichele and Falcon-Lang (2011). This "Permian Pompeii" gives insights into a spatially restricted forested lowland environment that sheltered dense hygrophilous vegetation dominated by medullosan seed ferns, tree ferns, cordaitaleans, conifers, and calamitaleans (Feng et al. 2012; Rößler et al. 2012a, 2014). Since 2012, a second excavation site in Chemnitz–Sonnenberg depicts another window into this fossil forest, providing new taphonomic and site-specific insights.

The exceptional preservation of this T^0 assemblage resulted from rapid in situ burial by proximal ejecta of the Zeisigwald Tuff pyroclastics (ZTP) as part of the Zeisigwald Volcanic Complex. In contrast to the well-investigated biotic aspects of the fossil forest, knowledge on the embedding pyroclastics remained on its state of the art for decades (Fischer 1990; Eulenberger et al. 1995). Besides practical use of reproducible stratigraphic correlation within the Chemnitz Basin, only minor attention was previously paid to volcano- and magma-genetic development of the Zeisigwald Volcanic Complex (Rank and Pälchen 1989; Fischer 1991). Retrospectively, geochemical and mineralogical composition of the pyroclastics had a crucial impact on both preservation and taphonomic specifics of the Chemnitz Fossil Forest, e.g., presence of fluorite as petrifaction agent (Rößler et al. 2012a). Resulting from initial taphonomic observations (Rößler et al. 2008, 2009, 2010), the demand for a thorough process analysis and reconstruction of the eruption arose, e.g., by comparison with insightful actual geology comparisons (Hoblitt et al. 1981; Swanson et al. 2013).

This contribution aims to provide a multi-disciplinary characterisation of the Zeisigwald Volcanic Complex, encompassing facies analysis based on high-resolution sedimentological and lithofacies data, a new radiometric age, as well as whole-rock geochemical and zircon Hf isotope analyses. By interrelating sedimentological and geochemical data, a new facies model of the Zeisigwald Tuff pyroclastics is presented, which builds up the basis for further taphonomic studies on the Chemnitz Fossil Forest. Results of both whole-rock geochemistry and zircon grain analyses allow new insights into magma origin and development of the Zeisigwald Volcanic Complex in context of the late post-Variscan magmatic activity in Central Europe.

Stratigraphy and geological setting

The Chemnitz Fossil Lagerstätte is located in the central part of the NE branch of the Chemnitz Basin, which represents a 70×30 km wide sedimentary depression between the Granulite Massif and the Erzgebirge Mountains (Fig. 1). Superposing deposits of small Carboniferous basin structures as well as Variscan folded metamorphic basement, the sedimentary succession of the Chemnitz Basin consists of 1550 m-thick early-to-late Permian (Asselian to Lopingian) continental red bed strata, which are subdivided into four formations based on sedimentary meso-cycles (Schneider et al. 2012) (Fig. 1).

The ZTP are part of the Leukersdorf Formation, which is of late Sakmarian-to-early Artinskian age, based on biostratigraphic data from sporomorphs and radiometric dating (Rößler et al. 2009; Schneider et al. 2012; Schneider and Scholze 2016), and represents the third of four formations in the Chemnitz Basin (Fig. 2). The Leukersdorf Fm. consists of approximately 800 m-thick sedimentary and volcanic deposits dominated by wet red beds of an alluvial fan/alluvial plain/lake system. Silty-to-sandy fine clastics of the alluvial floodplain were deposited in front of semi-arid-type alluvial fans and are intersected by conglomerates of shallow-braided channels (Schneider et al. 2012). These deposits are differentiated into three fining-up meso-cycles with minor palustrine–lacustrine deposits at their tops. The nearly basin-wide distributed lacustrine Reinsdorf Horizon on top of the second meso-cycle correlates with the ceasing Late Sakmarian/Early Artinskian wet phase D of Roscher and Schneider (2006). Common vertisols, calcisols, and remains of predominantly meso-to-xerophilous floral elements indicate increasing seasonality with prominent dry phases (Schneider et al. 2012). The recurrence of hygrophilous elements

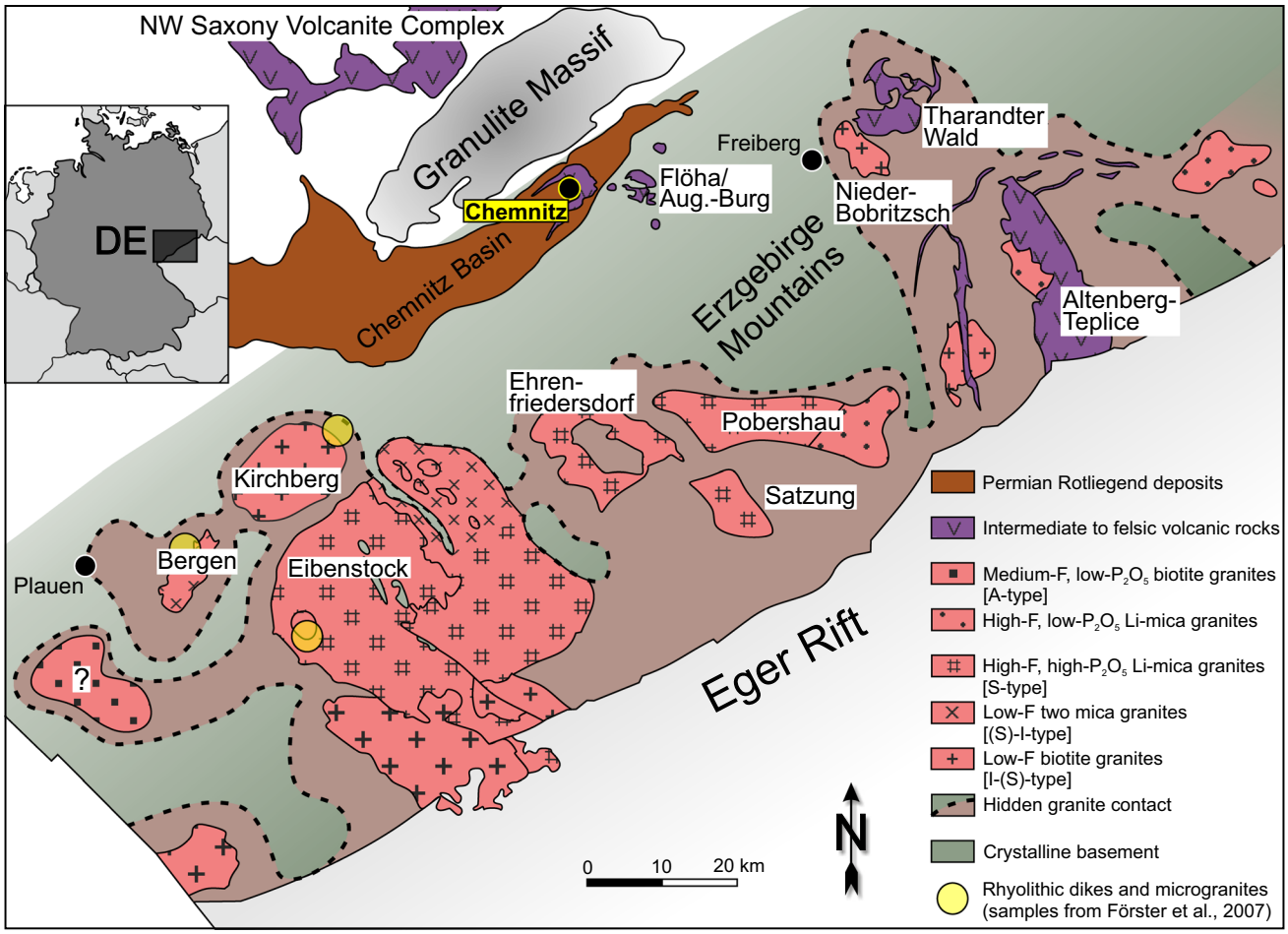

Fig. 1 Geographic position and geological map of southern Saxony showing the late-variscid magmatic granitoides and volcanites of the major geological units surrounding the Chemnitz Basin and the working area in Chemnitz (modified from Förster et al. 1999, 2007 and; additional data from; Schneider et al. 2012)

in the Chemnitz Fossil Forest is probably locally restricted to a basin-central "wet spot" ecosystem sensu DiMichele et al. (2006), at this stratigraphic level in the Chemnitz Basin. The ecosystem was once growing under strong seasonal conditions of monsoonal climate, which is indicated by mineralogical characteristics of the palaeosol and annual tree rings in woody plants (Luthardt and Rößler 2017; Luthardt et al. 2016, 2017) (Fig. 2).

With its growing significance, the necessity to establish the Chemnitz Fossil Lagerstätte as a reliable milestone in global correlation schemes (Schneider and Scholze 2016) steadily increases and requires a strong age constraint. The biostratigraphic position of the fossil forest is shown by several methods: amphibian remains of the *Melanerpeton pusillum–Melanerpeton gracile* Zone indicate a position in the European highest Lower Rotliegend (Werneburg and Schneider 2006; Schneider and Werneburg 2012). Macrofloral remains do not provide sufficiently precise results, but largely indicate an early Permian age. A stratigraphic position in the latest Asselian has been supported by a rich palynoflora dominated by the saccate pollen taxa *Potonieisporites* spp., *Florinites ovalis*, and *Vesicaspora* spp., and by *Vittatina* sp. from the palustrine Rottluff Coal in the lower part of the Leukersdorf Fm. (Döring et al. 1999). This association shows great similarities with palynological data of the sporomorph zone XVI, level S4, uppermost Slavjanskaja Svita of the Donetsk Basin reference section.

The Zeisigwald Volcanic complex

Permo-Carboniferous magmatism in the Saxo-thuringian zone initiated at ca. 330 Ma and is mainly related with late-to-post-orogenic crustal transpression/extension after the major collisional phase of the Variscan Orogeny (Kroner and Romer 2013). Volcanic activity in the study area arose in the Moscovian by the eruption of felsic pyroclastics of the neighbouring Flöha Volcanic Complex at ca. 310 Ma (Löcse et al., under review). Several major fault systems as

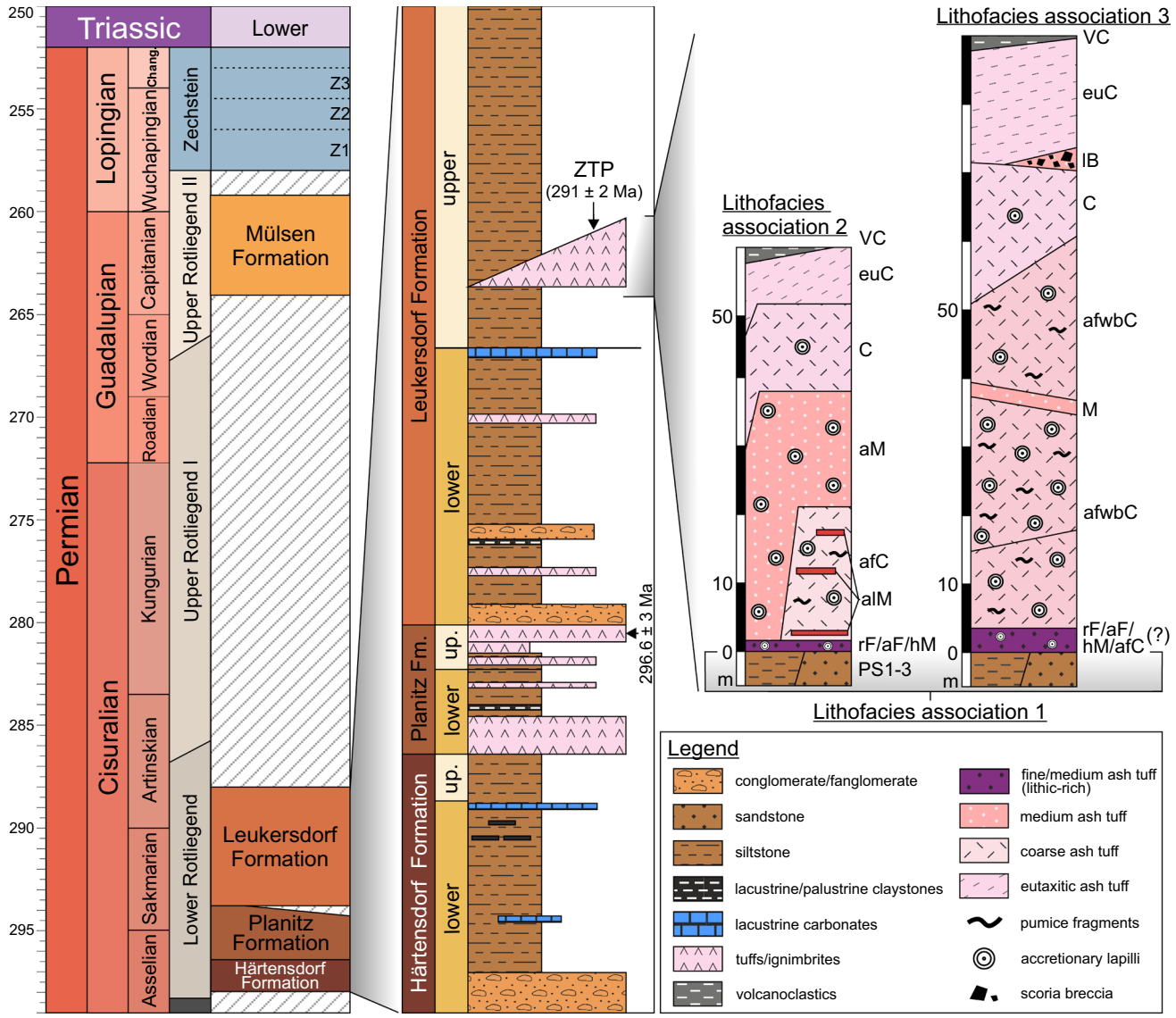

Fig. 2 Stratigraphic position of the ZTP within the Rotliegend Chemnitz Basin (after Schneider et al. 2012; isotopic age of 296.6 ± 3 Ma by; Hoffmann et al. 2013) and ZTP schematic profiles of lithofacies associations (LA) 1 to 3, whereas LA 1 represents underlying sediments of the Upper Leukersdorf Fm. and LA 2/3 are of pyroclastic origin

the WSW–ENE-trending Central Saxonian lineament, the WNW–ESE-trending Gera-Jáchymov, and the NNW–SSE-trending Leipzig-Regensburg fault zones were potential pathways for magma rise (Schneider et al. 2012). In the Chemnitz Basin, volcanism initiated during sedimentation of the upper Härtensdorf Fm. by several felsic eruptions, cumulated in the Planitz Fm. represented by mafic-to-intermediate ejecta, which show transition to increasing felsic character and terminated with eruption of the ZTP in the upper Leukersdorf Fm. (Fig. 2).

Ejecta of the Zeisigwald Volcanic Complex are widely distributed in the NE branch of the Chemnitz Basin and mainly covered by the settlement area of Chemnitz. Following the NE–SW trend of the basin branch, pyroclastics build up a ca. 10 km elongated deposit with a maximum thickness of ca. 90 m in the Zeisigwald area (Eulenberger et al. 1995). Volcanic ejecta are exclusively of pyroclastic origin, resulting from explosive volcanism of felsic magma. Altogether, an erupted tephra volume of around 8 km^3 was roughly estimated by Fischer (1991), suggesting a Volcanic Explosivity Index of VEI 5 (very large eruption, after Newhall and Self 1982) and an eruption magnitude of M 5–6 (Mason et al. 2004), which is comparable to the last major eruption of Mt. St. Helens (Cascade Range, Washington State, USA), in 1980 (Hoblitt et al. 1981; Waitt 1981). However, in comparison with the large volcanic complexes of

North Saxony (Wurzen Caldera: M8; Repstock et al. 2017) and Altenberg-Teplice (e.g., Breiter et al. 2001), it represents a rather small volcanic event.

For the first time, the ZTP was investigated in more detail by Fischer (1990, 1991) who developed a stratigraphic model mainly based on drill core data. The model differentiates four major pyroclastic horizons/sequences (*b, a*$_{1/2}$, s_o/s_c, ign, re), each representing a certain eruption phase (Fischer 1990; Eulenberger et al. 1995; Rößler et al. 2008). Hence, the ZTP is interpreted as product of a multi-staged plinian eruption of predominantly phreatomagmatic character, whereas the ascending magma escaped explosively from a fissure by coming into contact with surface-near groundwater. Later, Eulenberger et al. (1995) interpreted a ring-shaped, fault-bounded structure in the Zeisigwald area as a trapdoor caldera. However, the initiation of the two scientific excavations in Chemnitz–Hilbersdorf and Chemnitz–Sonnenberg revealed new data on the basal ZTP horizons challenging the existing concepts.

The first radiometric dating performed by Nasdala et al. (1998) yielded an age of 278 ± 5 Ma, which is, however, in considerable dissent to biostratigraphic data. In 2009, a second dating by SHRIMP technology on zircons from the Chemnitz–Hilbersdorf excavation was undertaken, providing an U/Pb age of 290.6 ± 1.8 Ma (Rößler et al. 2009).

Material and methods

Data collected for more than 30 years from temporary outcrops and drillings in the settled area of Chemnitz (Fischer 1991; Eulenberger et al. 1995) are used as basis for the revised lithofacies concept. New data on sedimentology, whole-rock, U–Pb zircon ages and isotopic geochemistry originate from both excavation sites in Chemnitz–Hilbersdorf (N 50°51 × 9.85″, E 12°56 × 45.95″) and Chemnitz–Sonnenberg (N 50°50 × 7.74″, E 12°56 × 2.06″), as well as from the Zeisigwald area in the NE of Chemnitz (N 50°51 × 8.19″, E 12°57 × 50.16″) and additional outcrops (Fig. 3).

Sedimentology and lithofacies concept

New data and finds from the excavations required in part re-evaluation and re-interpretation of the existing facies model of Fischer (1991), who classified pyroclastic horizons based on their stratigraphic occurrence. In this study, however, these pyroclastic horizons or sub-horizons are described as lithofacies, which are distinguished by unique compositional and textural features (Cas and Wright 1987; Sulpizio et al. 2007; Brown et al. 2009). Lithofacies associations are established to combine pyroclastic deposits with regard to their spatial distribution, stratigraphic occurrence, and significance during the eruption process. Grain size nomenclature of pyroclastic horizon follows the classification provided by Sohn & Chough (1989).

Whole-rock geochemistry

Five samples were taken from the Chemnitz–Hilbersdorf excavation and three samples from the Chemnitz–Sonnenberg excavation from different lithological (sub-)units (Fig. 7), whereas each sample encompasses 1–3 kg rock material. Further five samples originate from localities 3 + 4 (Fig. 3). Whole-rock samples were prepared by the standard methods and analysed using FUS-ICP/FUS-MS and INAA to detect major and trace-element concentrations. Raw data of Rare-Earth Elements (REE) were normalised by CI chondrite (McDonough and Sun 1995). Results are given in Table 2 (supplementary data).

U–Pb zircon ages of magmatic and inherited zircon

Sampling site for zircon grain analysis (sample VWC 1) is located in the northern corner of the excavation site ($X = 3.40$, $Y = 9.00$, $Z = 2.30$), close beneath the horizontally entombed cordaitalean trunk KH0025. It was attained from pyroclastics in the upper section of Unit S 3.

Zircon concentrates were separated from 2 to 4 kg sample material at the Senckenberg Naturhistorische Sammlungen Dresden using the standard methods. Final selection of the zircon grains for U–Pb dating was achieved by hand-picking under a binocular microscope. Zircon grains of all grain sizes, colours, and morphological types were selected, mounted in resin blocks, and polished to approximately half of their thickness.

Zircons were analysed for U, Th, and Pb isotopes by LA–SF–ICP–MS techniques at the Senckenberg Naturhistorische Sammlungen Dresden (Museum für Mineralogie und Geologie, Sektion Geochronologie), using a ThermoScientific Element 2 XR sector field ICP-MS coupled to a New Wave UP-193 Excimer Laser System. A teardrop-shaped, low volume laser cell constructed by Ben Jähne (Dresden) and Axel Gerdes (Frankfurt/M.) was used to enable sequential sampling of heterogeneous grains (e.g., growth zones) during time-resolved data acquisition. Each analysis consisted of 15 s background acquisition followed by 30 s data acquisition, using a laser spot size of 25 and 35 µm, respectively. Measurements were done with a repetition rate of 10 Hz and an energy density of 5–6 J/cm^2. A common-Pb correction based on the interference- and background-corrected ^{204}Pb signal and a model Pb composition (Stacey and Kramers 1975) was carried out if necessary. The necessity of the correction is judged on whether the corrected ^{207}Pb/^{206}Pb lies outside of the internal errors of the measured ratios. Raw data were corrected for background

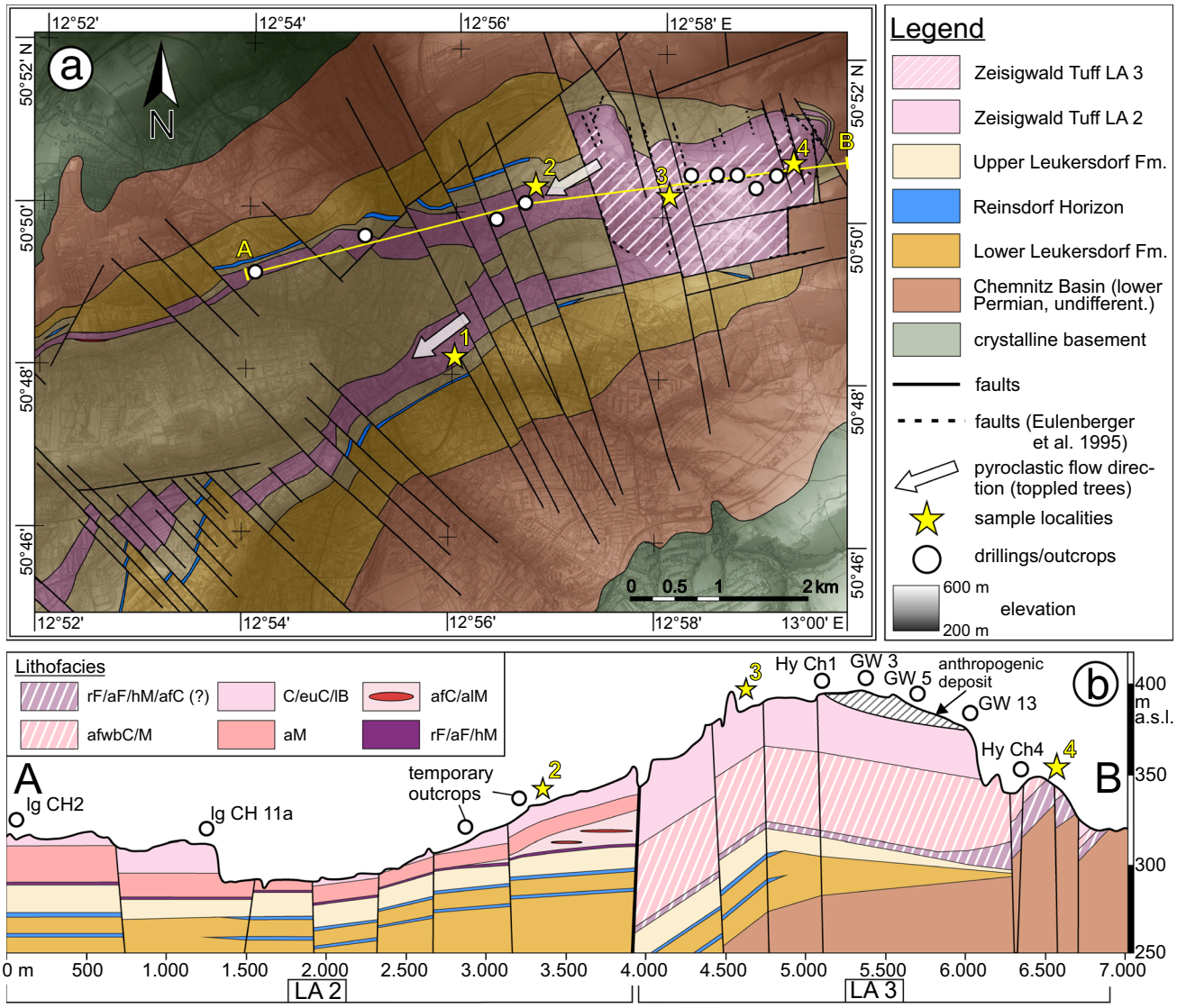

Fig. 3 Geology of the Zeisigwald Volcanic Complex. **a** Geological map showing part of the NE Chemnitz Basin in the settled area of Chemnitz and distribution of the ZTP: eruption centre is assumed to be located somewhere north of the white striated area of LA 3; Outcrops and sample localities: 1 Chemnitz–Sonnenberg excavation; 2 Chemnitz–Hilbersdorf excavation; 3 Findewirth quarry; 4 Naundorfer Delle quarry; drillings represent a selection of available data, which were used to interpolate geologic underground of profile section A–B. **b** Schematic section A–B from "a" showing supposed spatial architecture of the ZTP lithofacies from N to W, interpolated from drillings; vertically exaggerated by factor 2.5

signal, common-Pb, laser-induced elemental fractionation, instrumental mass discrimination, and time-dependant elemental fractionation of Pb/Th and Pb/U using an Excel® spreadsheet program developed by Axel Gerdes (Institute of Geosciences, Johann Wolfgang Goethe-University Frankfurt, Frankfurt am Main, Germany). Reported uncertainties were propagated by quadratic addition of the external reproducibility obtained from the standard zircon GJ-1 (~0.6% and 0.5–1% for the $^{207}Pb/^{206}Pb$ and $^{206}Pb/^{238}U$, respectively) during individual analytical sessions and the within-run precision of each analysis. A secondary standard (Plesovice) was used for calibration of our primary standard (GJ-1) at regular intervals, using a laser spot size of 35 µm. Repetitive measurements of the Plesovice zircon resulted in an age of ca. 337 Ma, which is in accordance with the results of Sláma et al. (2008).

Concordia diagrams (2σ error ellipses) and concordia ages (95% confidence level) were produced using Isoplot/Ex 2.49 (Ludwig 2001) and frequency and relative probability plots using AgeDisplay (Sircombe 2004). Discordant analyses were generally interpreted with care. The $^{207}Pb/^{206}Pb$ age was taken for interpretation for all zircons > 1.0 Ga, and the $^{206}Pb/^{238}U$ ages for younger grains. For further details on the analytical protocol and

data processing, see Gerdes and Zeh (2006) and Frei and Gerdes (2009). Zircons showing a degree of concordance in the range of 97–100% in this paper are classified as concordant because of the overlap of the error ellipse with the concordia. Th/U ratios are obtained from the LA–ICP–MS measurements of investigated zircon grains. U and Pb contents and Th/U ratio were calculated relative to the GJ-1 zircon standard and are accurate to approximately 10%. Analytical results of U–Th–Pb isotopes and calculated U–Pb ages are given in Table 1 (supplementary data). Stratigraphic ages have been taken from the International Chronostratigraphic Chart v2017/02 (Cohen et al. 2013; updated).

Lu–Hf isotopes of magmatic zircon

Hafnium isotope measurements on zircons of sample VWC 1 were performed with a Thermo-Finnigan NEPTUNE multi collector ICP-MS at the Goethe Universität Frankfurt (GUF, Institut für Geowissenschaften, Fachbereich Mineralogie) coupled to a RESOlution M50 193 nm ArF Excimer (Resonetics) laser system following the method described in Gerdes and Zeh (2006, 2009). Spots of 40 µm in diameter were drilled with a repetition rate of 5.5 Hz and an energy density of 6 J/cm^2 during 50 s of data acquisition. The instrumental mass bias for Hf isotopes was corrected using an exponential law and an $^{179}Hf/^{177}Hf$ value of 0.7325. In case of Yb isotopes, the mass bias was corrected using the Hf mass bias of the individual integration step multiplied by a daily βHf/βYb offset factor (Gerdes and Zeh 2009). All data were adjusted relative to the JMC475 of $^{176}Hf/^{177}Hf$ ratio = 0.282160 and quoted uncertainties are quadratic additions of the within-run precision of each analysis and the reproducibility of the JMC475 (2SD = 0.0028%, $n = 8$). Accuracy and external reproducibility of the method were verified by repeated analyses of reference zircon GJ-1 and Plesovice (Table 4: supplementary data). Results are in perfect agreement with previously published results (e.g., Gerdes and Zeh 2006; Sláma et al. 2008) and with the LA–MC–ICP–MS long-term average of GJ-1 (0.282010 ± 0.000025; $n > 800$) and Plesovice (0.282483 ± 0.000025, $n > 300$) reference zircon at GUF.

The initial $^{176}Hf/^{177}Hf$ values are expressed as εHf(t), which is calculated using a decay constant value of $1.867 \times 10–11$ year^{-1}, CHUR after Bouvier et al. (2008; $^{176}Hf/^{177}Hf_{CHUR,today} = 0.282785$ and $^{176}Lu/^{177}Hf_{CHUR,today} = 0.0336$) and U–Pb and Pb–Pb ages obtained for the respective domains (Table 4: supplementary data). For the calculation of Hf two-stage model ages (T_{DM}) in billion years the measured $^{176}Lu/^{177}Lu$ of each spot (first stage = age of zircon), a value of 0.0113 for the average continental crust and a juvenile crust $^{176}Lu/^{177}Lu_{NC} = 0.0384$ and $^{176}Hf/^{177}Hf_{NC} = 0.283165$ (average MORB; Chauvel et al. 2008) was used.

Results

Volcanic ejecta of the Zeisigwald Volcanic Complex are exclusively of pyroclastic origin. Nevertheless, they provide considerable implications on magmatic processes, which are constrained by geochemical results of element and isotopic compositions. Several lithofacies show specific trace-element compositions and trends, which are significant for stratigraphic and taphonomic purposes, but also offer insight into magma origin and evolution.

Lithofacies

Altogether, 12 lithofacies of pyroclastic origin are distinguished (Table 1). Besides pyroclastic units, three lithofacies of alluvial floodplain deposits (PS 1–3) are described, directly underlying the ZTP (Table 1). As these predominantly clastic sediments once represented the ancient palaeo-surface and substrate of the Chemnitz Fossil Forest, they are part of the T^0 assemblage and, therefore, integrated into the facies model.

Lithofacies PS 1–3

Description: The epiclastic sedimentary succession of lithofacies PS 1 was exposed in the excavation of Chemnitz Hilbersdorf. It represents a 1.85 m-thick horizon of silt-to-medium sand, which is red-coloured in the upper section and light green bleached in the lower section. Carbonate and haematite nodules occur, as well as a decimetre-thick layer of massive carbonate blocks. This lithofacies supported the dense hygrophilous vegetation of the fossil forest and shows many fossil roots, but also animal remains (Dunlop et al. 2016) in their uppermost part.

Lithofacies PS 2 is described from the Chemnitz–Sonnenberg excavation and represents a ca. 1.00 m-thick horizon of clay to siltstone. The upper section is of light greyish-green colour and strongly silicified. The lower section is dark grey and shows greenish to purple mottling. Fossil roots are rare and restricted to the uppermost part.

Lithofacies PS 3 is recognised as clay to siltstone of light-purple colour with light grey bleached areas, which is in part strongly silicified. Many fossil roots occur and are predominantly preserved as mould casts. Preliminary geochemical results point to a pyroclastic composition, as it shows pattern of REE concentrations similar to the overlying pyroclastics of the ZTP.

Interpretation: Lithofacies PS 1 is interpreted as a clastic, well-drained less mature palaeosol, which developed under monsoonal palaeoclimate and was influenced by a high and stable groundwater table (Luthardt et al. 2016). Lithofacies PS 2 is assumed to have once been a clastic, weakly

Table 1 Overview of lithofacies, their interpretation, association, and synonyms used in excavation and in the previous studies (Eulenberger et al. 1995)

Lithofacies	Description	Geochemical fingerprint	Interpretation	Eruption energy	Lithofacies association	Chemnitz–Hilbersdorf excavation	Chemnitz–Sonnenberg excavation	Eulenberger et al. (1995)
VC	Clastic sediment, interbedded or mixed with ash tuff layers, channel erosion and trough cross-bedding	-	Re-deposited/reworked volcanoclastics		2/3	–	–	res
lB	Scoria breccia, fine ash tuff matrix, in situ brecciation of glass fragments, locally restricted	-	Lag fall deposit	High	3			a_2
euC	Coarse-grained ash tuff, eutaxitic texture (fiamme), lithic lapilli, massive	High Zr/Ti	Hot concentrated flow deposit (magmatic, minor phreatomagmatic)					ign_3
C	Medium- to coarse-grained ash tuff, pumice and lithic lapilli, (rarely accretionary lapilli), poorly sorted, massive							ign_1
afwbC	Coarse-grained ash tuff, pumice and accretionary lapilli, poorly sorted, wavy bedding, fluorite concretions	High F + Y	High-energy concentrated flow deposit (phreatomagmatic)	Very high				s_f
M	Medium-grained ash tuff, moderately sorted, massive	–						s_f
aM*	Medium-grained ash tuff, accretionary lapilli, well to moderately sorted, poorly stratified, fossil stems and branches at the base	–	Surge-like diluted flow deposit (phreatomagmatic)	High	2		LE 3	s_o
alM*	Medium-grained ash tuff, accretionary lapilli, crystals, well to moderately sorted, massive, silicified	–	Flow-associated ash cloud deposit	Low to medium		S 4	–	–
afC*	Coarse-grained ash tuff, many pumice and lithic lapilli, accretionary lapilli, poorly sorted, massive, fossil stems and branches at the base	High F + Y	Concentrated flow deposit (spatially restricted, phreatomagmatic)			S 5.4, S 3	–	a_1
hM*	Medium-grained ash tuff, moderately sorted, many lithic and pumice lapilli, horizontally bedded, coarsening-up, fossil plant remains	–	Fallout deposit from ash cloud with lateral transport component (surge-like, phreatomagmatic)			S 5.2/0.3	LE 2c/d	*b*
aF*	Fine-to-medium-grained ash tuff, accretionary lapilli, well to moderately sorted, indistinct bedding of slightly coarser layers, fossil plant and animal remains	–				S 5.1	LE 2b	
rF*	Fine-grained ash tuff, very well sorted, massive, micro-relief compensating, fine rooted	Low SiO_2, high Zr	Ash fall deposit	Very low		S 5.0	LE 2a	
PS 1	Densely rooted sandstone, red-coloured, carbonate concretions	–	Clastic palaeosol of alluvial floodplain	–	1	S 6	–	–
PS 2	Sparsely rooted mudstone, light-green-coloured, silicified	–	Clastic palaeosol of alluvial floodplain			–	LE 1	
PS 3	Densely rooted mudstone, purple-coloured, partly silicified	–	(Pyro)clastic palaeosol			–	–	

*Fossiliferous horizons

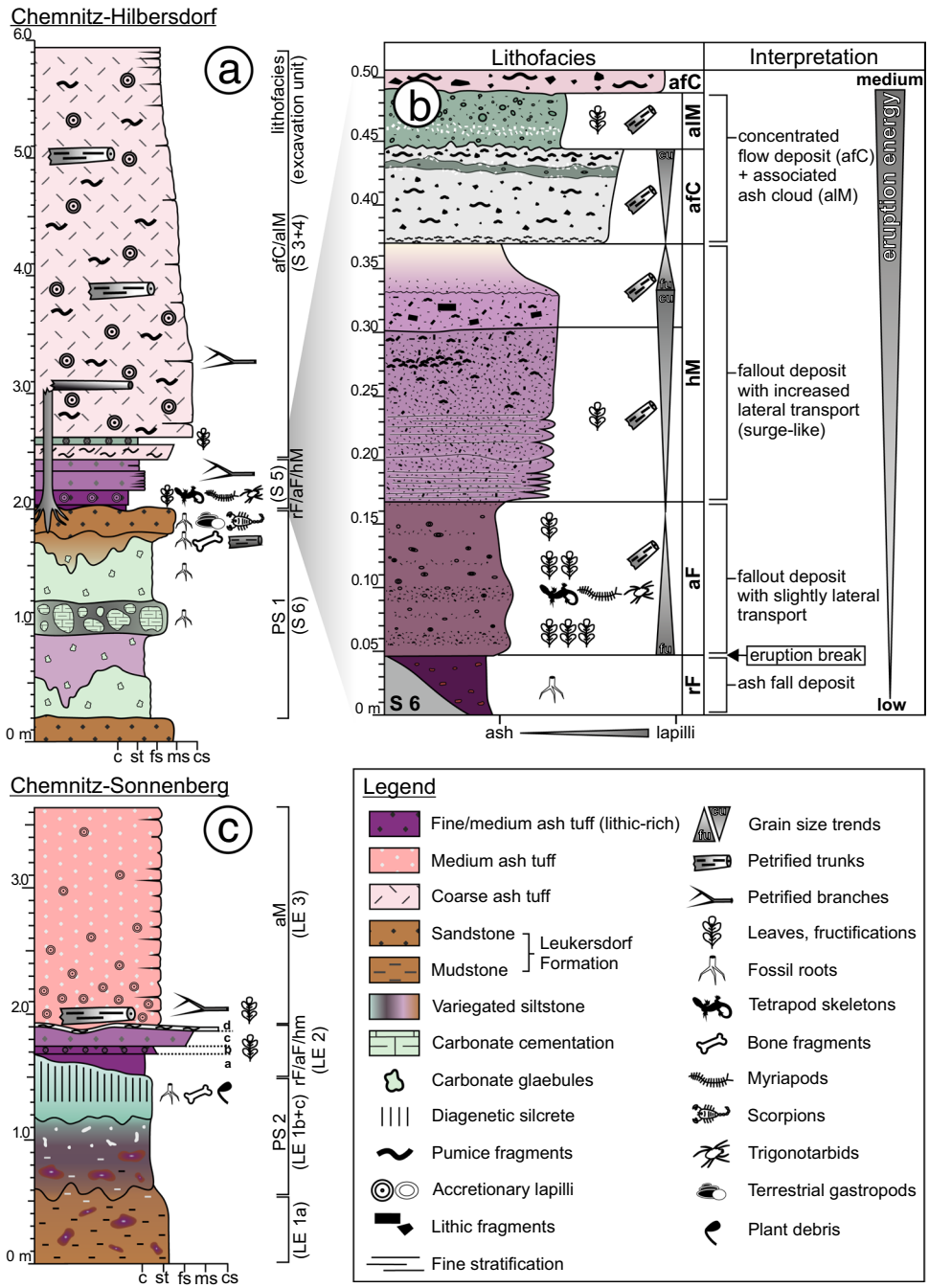

Fig. 4 Detailed lithology and sedimentology of the basal pyroclastics and their interpretation. **a** Excavation profile of Chemnitz–Hilbersdorf; **b** detailed profile section of most basal pyroclastics; **c** excavation profile of Chemnitz–Sonnenberg; colours in sketch are close to original colours in outcrops

developed, poorly drained palaeosol supporting the fossil forest vegetation at a wet locality (Luthardt et al. 2016). Lithofacies PS 3 represents another palaeosol type, which was recently discovered near the Chemnitz–Hilbersdorf excavation. If this palaeosol is of pyroclastic origin, it could point to a minor eruption several years before the major eruption.

Lithofacies rF

Description: The lithofacies represents an up to 0.20 m-thick, dark purple, fine-grained ash tuff, which is mostly delithified and partly bleached due to alteration. It contains many microscopic pumice fragments of 1–2 mm size, angular-to-sub-angular lithic fragments, idiomorphic quartz crystals of double-pyramidal habitus, few thick-walled glass shards and muscovite. Fabric is matrix-supported and massive to horizontally bedded. Thickness varies, because the horizon compensated the morphological relief of the palaeosol surface (Fig. 4). In general, this lithofacies is thicker distally, at the Chemnitz–Sonnenberg site (< 0.20 m) than proximally, at the Chemnitz–Hilbersdorf site (< 0.06 m). Small plant axes occur frequently and were identified as fine, predominantly

horizontally orientated former roots. In the Chemnitz–Hilbersdorf excavation, several leaf adpressions were found on the top of the lithofacies.

Interpretation: With regard to small grain size and good sorting, this lithofacies represents an ash fall deposit of a low-energy eruption event. The relief-filling distribution could be referred to post-depositional transportation processes by wind and/or surface water. Previously regarded as part of the b horizon (Fischer 1991), recent excavations revealed that this ash fall deposit probably predated the overlying pyroclastic deposits in a scale of weeks or months, which is indicated by initial rooting.

Lithofacies aF and hM

Description: Lithofacies aF is characterised as a purple–red, well sorted, non-welded, accretionary lapilli-bearing fine-grained ash tuff with coarser laminae (Figs. 4, 5a; compare also Spindler et al. 2018). Fabric is matrix-dominated and shows indistinct sub-horizontal bedding indicated by coarser laminae. Components are lithic fragments, predominantly blocky and rarely thin-walled shards as well as flattened pumice fragments of ca. 0.5 mm size. Accretionary lapilli frequently occur with diameters of 2–5 mm. In the Chemnitz–Hilbersdorf excavation (Unit S 5.1), lithofacies aF is approximately 0.12–0.20 m thick and contains large quantities of plant adpressions in the lowermost sections, such as leafy shoots, pinnate frond portions, and detached whole and fragmentary leaves reflecting both in situ and transported vegetational elements (Rößler et al. 2012b; Luthardt et al. 2016). Few centimetres above, faunal remains as the first arboreal varanopid pelycosaurs (Spindler et al. 2018), an aistopod lepospondyle, and remains of a probably new temnospondyle are preserved. Furthermore, several invertebrates were found, such as diplopods, one leg of *Arthropleura*, and several arachnids including trigonotarbids and one uropygid (Rößler et al. 2012b; Dunlop and Rößler 2013). In the Chemnitz–Sonnenberg excavation (Unit LE 2b), this lithofacies is 0.05–0.06 m thick and exhibits coarser laminae, similar to Unit S 5.1. Lithofacies aF has a wide distribution within the Zeisigwald Volcanic Complex and shows a strikingly constant thickness. Transition to lithofacies hM is continuous.

Lithofacies hM depicts a purple to light-purple, medium-grained and moderately sorted ash tuff, which is rich in lithic and pumice fragments. Lithic fragments are of metamorphic lithology and up to 6 mm in size. Pumice lapilli are flattened and measure up to 12 mm. Matrix consists of blocky-to-thin-walled shards. Fabric is matrix-supported and characterised by mm-scaled horizontal stratification at the base. In general, lithofacies hM shows a coarsening-up. In the Chemnitz–Hilbersdorf excavation (S 5.2/5.3), it has a distinct fining-up at the top. Thickness is about 0.21–0.32 m in the Chemnitz–Hilbersdorf excavation and about 0.20 m in the Chemnitz–Sonnenberg excavation. Spatial distribution is similar to lithofacies aF.

Interpretation: Both lithofacies aF and hM reflect a continuous depositional event. Accretionary lapilli and ash pellets, well sorting, horizontal stratification, and wide spatial distribution are indicative for a wet phreatoplinian fallout deposit (Self and Sparks 1978; Self 1983). The high amount of lithic fragments especially in lithofacies hM is interpreted as a result of vent-near accidental fragmentation of bedrock during the phreatomagmatic explosion (Cas and Wright 1987). In the Chemnitz–Hilbersdorf excavation site, a lateral transport component is evidenced by plant taphonomic indications (Rößler et al. 2009). In proximal areas, hybrids of ash fall deposits with flow components are reported to originate from asymmetric collapse of the pyroclastic column (Carey et al. 1988). However, due to the wide distribution with more or less the same thickness, a pure ash fall deposit is favoured and lateral transport could be explained by accompanying proximal downwind from the plume (e.g., Allen and Cas 1998). Reverse gradation in lithofacies hM and increase of lithic fragments could indicate enhancing eruption energy or vent-widening by wall erosion as suggested by Wilson et al. (1980). Both lithofacies have a high potential for detailed, but mainly adpression to cast preservation of plant and animal remains. Detailed preservation seems to reflect deposition temperatures distinctly below 50 °C.

Lithofacies afC and alM

Description: Lithofacies afC is characterised as a massive layer of light-red to purple-red, poorly sorted, matrix-supported and unwelded coarse-grained ash tuff with large sub-angular pumice lapilli (15–200 mm in diameter), abundant accretionary lapilli up to 12 mm in size, and minor amount of lithic fragments (Figs. 4b, 5b). In drill cores, it has a maximum thickness of 25 m (Eulenberger et al. 2010), which rapidly decreases to zero in northern and western direction from the Zeisigwald area. In the Chemnitz–Hilbersdorf excavation, it is represented as Unit S 3 and bears small-to-medium-sized upright-standing stems toppled at a height of about 1.5 m from the palaeosol surface. With regard to the spatially restricted distribution of this lithofacies, other trunks are supposed to be transported over small distances and are embedded horizontally in this layer with NE–SW orientation. Further phenomena of lateral transport are catchment areas, accretions of plant debris and large pumice fragments in the current shadow of densely standing upright trees (Rößler et al. 2012b). Bleaching haloes occurring around the petrified trunks and branches resulted from diagenetic processes that took place during the petrifaction of wood. One of the most famous fossils found in this layer is the so far largest anatomically preserved calamite

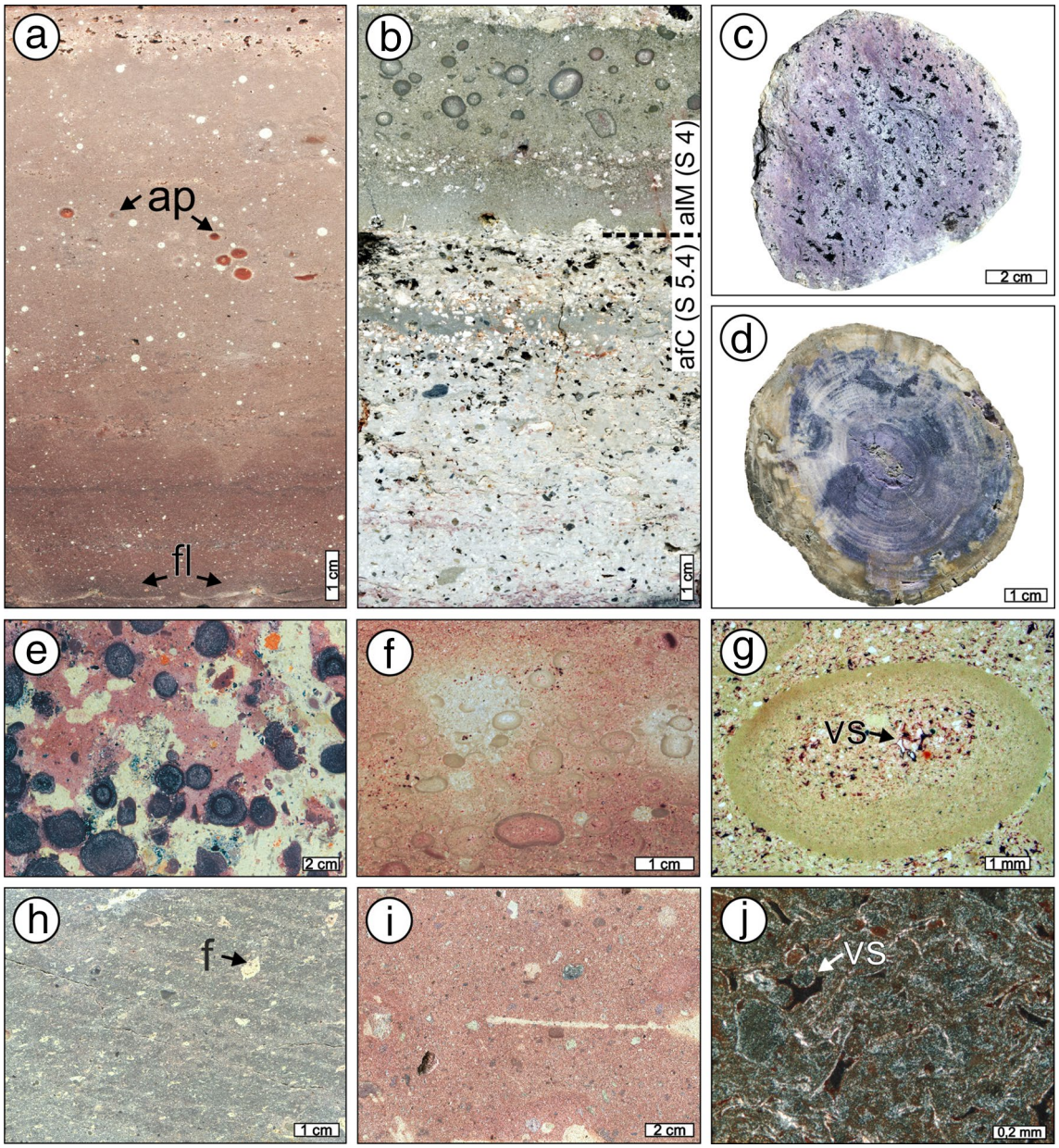

Fig. 5 Lithology of the ZTP. **a** Lithofacies aF representing the basal pyroclastic unit S 5.1 in the Hilbersdorf excavation profile (fl—fossil leafs in cross section; ap—ash pellets/accretionary lapilli); **b** lithofacies afC and alM (LA 2) representing units S 5.4 and S 4 in the Hilbersdorf excavation profile; c Fluorite nodule from the open pit in the Zeisigwald area (lithofacies afwbC) showing violet fluorite crystallising in pyroclastic ash; **d** petrified wood (*Agathoxylon* sp., K 5358, collection of MfNC) from the Hilbersdorf area preserved by violet fluorit as a unique feature of lithofacies afC; **e** large multi-rimmed accretionary lapilli in lithofacies afwbC from an open pit in the Zeisigwald area indicating high ash cloud turbulence and phreatomagmatic eruption style; **f** lithofacies aM of the Sonnenberg excavation profile with a concentration of accretionary lapilli in the basal part; **g** accretionary lapillus of lithofacies aM with thin-walled vesicular shards (vs) in its core giving evidence for phreatomagmatic formation; **h** welded facies of lithofacies euC with oriented fiamme (**f**) from the Zeisigwald area; **i** unwelded or slightly welded facies of lithofacies C found east of the Zeisigwals area; **j** matrix of lithofacies C under cross-polarised light showing thin-walled vesicular shards (vs) and flattened pumice fragments

(*Arthropitys bistriata*) with an approximate length of 15 m (Feng et al. 2012; Rößler et al. 2012a).

Lithofacies alM represents a grey–green, rarely light-red, moderately sorted, accretionary lapilli bearing, medium-grained ash tuff. In the Chemnitz–Hilbersdorf excavation (Unit S 4), it has a thickness of 0.02–0.08 m (Fig. 5b). Accretionary lapilli are predominantly well-preserved, but rarely fragmentary, and have diameters of 5–6 (max. 10) mm. Further components are altered feldspar crystals of 1–3 mm grain size and lithic fragments (0.2–0.5 mm).

Matrix is predominantly composed of thin-walled vesicular, but also thick-walled blocky shards of 0.3–0.8 mm size. Fabric is massive and matrix-supported. A component sorting occurs, whereas feldspar crystals are enriched in a layer at the base, but accretionary lapilli at the top. The matrix of Unit S 4 is silicified forming a strongly lithified distinct layer, which is fragmented into metre-sized slabs. In several profiles, lithofacies alM occurs as multiple thin and spatially restricted layers, which are intercalating lithofacies afC. Rarely, moderately preserved and non-oriented leaf adpressions can be found.

Interpretation: Characterised as a_1 horizon by Fischer (1991), lithofacies afC was previously studied only from drill cores and inapplicably interpreted as ash fall deposit (Eulenberger et al. 1995; Kretzschmar et al. 2008). The Chemnitz–Hilbersdorf excavation recently provided large-scale sections and for the first time plant taphonomic indications pointing to directed lateral transport of sizable stems and branches (Rößler et al. 2012b). Thus, lithofacies afC and alM are rather considered as a product of a moderate-energy concentrated pyroclastic current (lithofacies afC) with accompanying ash cloud (lithofacies alM), comparable to deposits observed after Mount St. Helens' 1980 eruption (Rowley et al. 1981). Grain size differences from afC to alM indicate the flow-boundary zone, whereas fine ash of lithofacies alM most likely elutriated from the coherently flowing pyroclastic material (e.g., Branney and Kokelaar 2002). Subangular shape of pumice lapilli and blocks points to short distant transportation. Particle sorting in alM indicates vertical fallout from the turbulent diluted ash cloud (Carey et al. 1988). Accretionary lapilli and thin-walled shards show high moisture content as result of another phreatomagmatic explosion. Probably, shortly after deposition, lithofacies alM was cemented by silica, and thus insusceptible to erosion by overlying pyroclastics (Rößler et al. 2012a). The deposit shows a spatial restriction to the proximal eruption area with a high-aspect ratio, probably due to low relief energy. Repeated occurrence of alM indicates multiple depositional events as the result of a pulsating eruption. Missing relicts of charcoalified wood on the one hand and indications of boiling/expanding cell fluids in woody trees on the other hand suggest a temperature of 100–350 °C for the entombing pyroclastic current (Mißbach 1973; Babrauskas 2001). Preservation potential was restricted to silicified stems or branches in lithofacies afC, whereas few leaf adpressions were preserved in lithofacies alM.

Lithofacies aM

Description: The light-purple-to-red-coloured, moderately sorted, accretionary lapilli bearing, medium-grained ash tuff is in wide parts bleached to light-green colour (Figs. 4c, 5f). It represents a massive pyroclastic horizon with a wide distribution west of the Zeisigwald area (Fig. 3b). Thickness varies between 5 m in proximal and < 3 m in distal position (Eulenberger et al. 1995). It is characterised by a laterally homogenous grain size distribution and indistinct horizontal bedding in the outcrop. Fabric is massive and matrix-supported, whereas the matrix is composed of devitrified thin-to-thick-walled, rarely blocky shards, crystals and minor lithic fragments (Fig. 5g). Accretionary lapilli frequently occur up to 10 mm in diameter (average 3–6 mm), whereas many of them are fragmented. From base to top, frequency of accretionary lapilli decreases and larger pumice lapilli become more frequent. In the Chemnitz–Sonnenberg excavation lithofacies, aM has a remaining thickness of 1.75 m (unit LE 3). A large petrified trunk with a maximum diameter of 0.60 m was found in horizontal position oriented in NE–SW direction (Rößler and Merbitz 2009), sunken into lithofacies hM (LE 2c) and finally buried by aM (LE 3). Few upright-standing plants were found, so far, broken during deposition of aM. Moreover, many poorly preserved branches and twigs (petrifications and casts) were found at the base of aM (LE 3), as well as rare fragments of leafy shoots.

Interpretation: Fischer (1991) interpreted this horizon as base surge deposit in medial outflow facies (S_o), which he correlated with lithofacies afwbC (S_f) regarded as filling facies based on the caldera model. Uprooted trees are found slightly sunken in the preceding fallout deposits of ahM probably indicating an initial, high-energy lateral blast. Bark damage caused by grain blasting is frequently noted from pyroclastic density currents (Major et al. 2013), but was not observed on stems in the Chemnitz–Sonnenberg excavation, so far. At this site, there was not recognised any distinct bedding, dune structures, or low-angle truncation indicating turbulent flow behaviour (Fisher 1979; Cas and Wright 1987), as well as wide grain size spectrum with a high amount of accidental lithic clasts. In contrast, lithofacies aM is a thick massive horizon, whereas typical base surge sequences are almost invariably composed of multiple, < 0.5 m-thick layers, indicating several eruption pulses (Schmincke et al. 1973). Massive facies is mostly reported from medial facies of wet surges (Wohletz and Sheridan 1979). The wet phreatomagmatic character of aM is demonstrated by frequently occurring accretionary lapilli as well as by blocky and vesicular shards. Accretionary lapilli are of the rim type with multiple layering and are tending to be indicative for fallout deposits (Schumacher and Schmincke 1991), but could also occur in pyroclastic flows (Brown et al. 2009, 2012). Moreover, base surge deposits usually have a proximal-to-medial distribution and wedge-shaped geometry rapidly decreasing in thickness from the vent (Cas and Wright 1987), whereas aM shows a wide distribution over ca. 10 km, slowly decreasing in thickness in distal position and mantling topography produced by lithofacies afC.

Altogether, sedimentological features observed for aM are more indicative for continuous fallout from a downwind plume (Cas and Wright 1987; Allen and Cas 1998). Significant destruction on arborescent vegetation and alignement of toppled large trees pointing to West has been recognised for more than a century in Chemnitz (Rößler 2001). This pattern is much likely referred to an initial air-borne shock wave produced by the phreatomagmatic explosion (Wohletz et al. 1984).

Lithofacies afwbC and M

Description: Lithofacies afwbC represents a yellowish white, light-purple mottled, poorly sorted and coarse-grained ash tuff, which has a thickness of 35–55 m (Figs. 2, 5e). Pumice lapilli and, in part, accretionary lapilli occur frequently, but lithic fragments are rare. Fabric is massive and matrix-supported. In outcrops, a characteristic wavy bedding with up to 10 m wave length and an amplitude of < 0.5 m is observed. Up to three depositional events are distinguishable, which are laterally interfingering and locally interrupted by lithofacies M. Lithofacies afwbC is spatially restricted to the Zeisigwald area (Fig. 3). Amount and size of accretionary lapilli vary among horizons, whereas the lower horizon is rich in up to 30 mm large, multi-rimed accretionary lapilli, the upper horizons exhibit few and smaller accretionary lapilli up to 15 mm size. Nodules rich in fluorite occasionally occur (Fig. 5c).

Lithofacies M is recognised as a bluish-purple, well sorted, fine-to-medium-grained ash tuff. It locally interfingers with lithofacies afwbC and has a varying thickness of few decimetres.

Interpretation: Lithofacies afwbC is interpreted as product of a series of high-energetic, predominantly diluted pyroclastic density currents resulting from a collapsed ash column. Highly turbulent flow processes are indicated by wavy bedding (Walker et al. 1981; Wilson 1985) and large accretionary lapilli. The latter reflect high moisture content of the ash, an indication of additional phreatomagmatic explosion. Comparably small grain size and minor grain size variations could point to a high degree of fragmentation (Cas and Wright 1987). The intercalated lithofacies M most likely represents the product of ash cloud sedimentation during a phase of quiescence. Altogether, a very proximal position to the eruption centre is assumed, which is referred to the high thickness with exceptionally steep facies gradients. Thickness variations and interfingering of the single horizons suggest a small depositional space.

Lithofacies C and euC

Description: Lithofacies C represents a light-red-coloured, poorly sorted coarse-grained ash tuff that shows secondary bleaching spots (Fig. 5i). It is composed of a coarse ash matrix of thick-walled, in part vesicular shards and pumice fragments (Fig. 5j). Non-collapsed pumice lapilli and accretionary lapilli are rare, but pumice swarms occur at the top of the lithofacies. Angular-to-sub-angular lithic fragments and tuff clasts are frequently recognised. Fabric is massive and matrix-supported. Thickness is highly variable, ranging between 1.5 and 33.5 m. Of all lithofacies, it shows the widest distribution in the areas east (Fig. 3a, outcrop 4) and west, but also within the Zeisigwald area, where it overlies lithofacies afwbC.

Lithofacies euC is a reddish-purple or greenish-grey, moderately sorted, coarse-grained ash tuff with eutaxitic fabric (Fig. 5h). Frequently occurring pumice lapilli are in wide parts transformed to fiamme, which show a distinct orientation. Moreover, lithic fragments and thick-to-thin-walled shards are recognised. The degree of welding decreases to the top and base, as well as laterally in southern direction. Thickness is highly variable, from 1.6 to > 14 m.

Interpretation: Both lithofacies C and euC are interpreted as products of a series of high-energy, diluted to concentrated pyroclastic density currents. In lithofacies association LA 3, lithofacies C shows wavy bedding typically occurring in surge deposits (Schmincke et al. 1973), whereas C and euC in lithofacies association LA 2 are massive, more tending to an ignimbritic flow deposit. In contrast to the hitherto described lithofacies, these deposits show low phreatomagmatic influence, because accretionary lapilli and blocky/vesicular shards are rare. Instead, eutaxitic texture points to a high temperature of > 550 °C for euC, which predominantly occurs north of and within the Zeisigwald area pointing to a very proximal position. By exhibiting the highest volume of all lithofacies, deposits of lithofacies C and euC mark the climax of the Zeisigwald eruption.

Lithofacies lB

Description: It represents a light-to-dark greyish breccia of glassy scoria fragments, which are embedded in a matrix of crystal-rich, fine-grained ash tuff. Scoria fragments are larger than 8 cm and show isometric shape and in situ brecciation. The ca. 3.5 m-thick deposit is locally restricted to a small region north of the Zeisigwald area and underlies lithofacies euC.

Interpretation: Lithofacies lB is interpreted as a co-ignimbritic breccia or lag fall deposit (Wright and Walker 1977; Rowley et al. 1981) and, therefore, indicating a position close to the eruption centre. Summarised with the welding

gradation of lithofacies euC, the position of the eruption centre is estimated north of the Zeisigwald area.

Lithofacies VC

By Fischer (1991) originally described as "re" horizon, lithofacies VC represents widely re-deposited pyroclastics of the underlying lithofacies. It shows sedimentological features of water transportation, such as minor channel erosion and trough cross-bedding, but also intercalation with several thin pyroclastic layers. In the western medial-to-distal outcrop area, up to decimetre-thick fossiliferous chert lenses occur, which yielded numerous remains of a post-volcanic recovery flora (Tunger and Eulenberger 2001). Lithofacies VC marks the termination of the Zeisigwald Tuff eruption.

Lithofacies associations

In the Zeisigwald Volcanic Complex, three lithofacies associations (LA) are distinguished. The sedimentary basement (LA 1) formed the ancient palaeo-surface and controlled the depositional architecture of the pyroclastics (Fig. 2). The pyroclastic lithofacies associations LA 2 + 3 differ with regard to their spatial distribution, whereas LA 2 extends over a wide area and LA 3 is restricted to the small Zeisigwald area.

Lithofacies association LA 1

LA 1 encompasses clastic sedimentary rocks of lithofacies PS 1–3, which directly underlie the basal pyroclastics of the Zeisigwald Tuff, and are part of alluvial floodplain wet red beds of the upper Leukerdorf Formation. Upon these sediments, the ecosystem of the Chemnitz Fossil Forest once started to develop and throve until its volcanic entombment. As having been exposed to alteration processes controlled by seasonal palaeoclimate and vegetation, lithofacies frequently exhibit characteristics of soil-forming processes (early diagenetic alteration, rooting, pedoturbation/bioturbation, colour mottling, formation of Ca carbonate and ferric glaebules) with a certain local heterogeneity. The latter is understood as the result of laterally varying site-specific conditions (e.g., groundwater level and exposition), which are usually controlled by geomorphic parameters as topography, lake level and drainage systems. Regarding topography there was so far no evidence found for higher relief energy in the sedimentological record. Thus, palaeo-surface on the alluvial floodplain is assumed to have been characterised by minor elevation differences. Indicated by loosely scattered and small-sized channel deposits, fluvial sedimentation is under-represented in LA 1 and probably played a minor role in the Chemnitz Fossil Forest environment. As indicated by lithofacies PS 1 and probably PS 2, the groundwater level is assumed to have been high (Luthardt et al. 2016).

Lithofacies association LA 2

Listed in the stratigraphic order from the base to the top, LA 2 comprises lithofacies rF, aF, hM, afC, alM, C, euC and VC. In general, the occurrence of LA 2 pyroclastics encompasses wide parts of the elongated, more or less oval-shaped ZTP distribution area (Fig. 3a) with a maximum thickness of ca. 47 m, which slightly decreases from NE (proximal) to SW (distal). Except hM/afC all lithofacies show low variation in thickness. All of these lithofacies represent at least three eruption phases, in part with pulsating character as indicated by repeated occurrence of lithofacies hM/afC in the profile. On the one hand, eruption phases reflect an increase of both eruption energy and erupted magma volume. On the other hand, a transition from wet, strongly phreatomagmatic influenced lithofacies (aF, aM) to dry and hot pyroclastics (lithofacies C) can be concluded. Plant taphonomic features in lithofacies afC and alM show "pyroclastic" transport from NE to SW, suggesting an eruption centre in north-eastern marginal position of the Zeisigwald Tuff deposits (Fig. 3a).

Lithofacies association LA 3

Transition between LA 2 and 3 is fault-generated at the western margin of LA 3 showing considerable vertical and probably horizontal displacement (Eulenberger et al. 1995). Within, but fault-bounded from LA 2, lithofacies association LA 3 covers a comparably small area of 2.2 × 1.2 km diameter, but exhibits a much higher thickness of up to 90 m (Fig. 3). Lithofacies M, afwbC, C, euC, lB and VC occur and represent deposits of turbulent pyroclastic currents with antidune structures (afwbC), eutaxitic fabrics (euC) and lag fall deposit (lB), suggesting close proximity to the eruption centre.

Whole-rock geochemistry

The ZTP exhibits a silica content of 72 to 84 wt%, thus showing a sub-alkaline rhyolitic composition in the TAS diagram (Fig. 6a). Lower SiO_2 portions down to 59 wt% in two of the samples from the Chemnitz–Sonnenberg excavation are the result of diagenetic overprint. Compared to average composition of the continental crust (Taylor and McLennan 1985), all samples possess major element depletion, particularly of CaO and Na_2O, but also of TiO_2, Fe_2O_3, MgO, and P_2O_5. Following the Shand's index (Maniar-Piccoli 1989), major elements of the ZTP show a strongly peraluminous composition. Trace-elemental composition is characterised by enrichment of trace elements, such as Li, Be, F, Rb, Y, Sn, Cs, Bi, U and Th, whereas most of them are classified as

incompatible. Particularly lithofacies afC (GP 469-1) shows a striking anomaly of enriched Yttrium and Fluorine, which led to unique fluorite petrification in fossil wood exclusively preserved in this horizon (Rößler et al. 2008). Otherwise, trace elements, such as Sr, Ba, Sc, V, Cr, Co, Ni and Zr are in many samples extremely depleted in all horizons. In the classification diagram of Pearce (1996), which is based on Winchester and Floyd (1977), the samples show a wide spread of the Zr/Ti and Nb/Y trace-element ratios reflecting an evolved, sub-alkaline rhyolitic to dacitic magma composition with a slight trend to intermediate, alkaline trachyandesitic and andesitic composition (Fig. 6b). After Whalen et al. (1987), magma composition of the ZTP was related to A-type granites with a slight tendency to I-/S-type granites. The Nb/Ta ratio of 3.8–9.6 is also regarded typical for A-Type granites (Green 1995). Granite discrimination plot for the tectonic setting (Pearce et al. 1984) shows Rb/Y + Nb compositions of syn-collisional to intraplate granites (Fig. 6 c).

The distribution pattern of REE shows high congruence of all samples (Fig. 6d) except of GP 469-1 (lithofacies afC), which has slightly higher concentrations of HREE (Heavy Rare-Earth Elements). The REE plots of all samples show a so-called bird-wing pattern, which is characterised by a distinct negative Europium anomaly and a slight positive trend towards concentrations of HREE (Fig. 6d; compare Förster et al. 2007). The Nb vs. Ta plot of Fig. 6e reveals a high degree of fractional crystallisation during magma evolution, which is similar to values of the Erzgebirge granitoids (Förster et al. 1999) and nearly as high as values of the rhyolitic dike system from the western Erzgebirge region (Förster et al. 2007). The Y/Ho and Zr/Hf ratios tend to lower Zr/Hf values as it is typical for granitoid intrusions in the Erzgebirge region (Fig. 6f).

Geochemical composition of selected major element concentrations and trace-element ratios vary among lithofacies and demonstrate significant trends within the profile (Fig. 7). Lithofacies afC is characterised by low Zr/Y (0.39) and Nb/Y (0.05) ratios, as the result of relatively increased portion of Y (and HREE; Y: 254 ppm). The same is obvious in lithofacies afwbC (Y: 140 ppm). This anomaly probably results from an increased occurrence of heavy minerals, such as garnet, xenotime and apatite, which are usually rich in HREE + Y and were deposited at the base of the density current. Further, in contrast to all other lithofacies of LA 2, an exceptionally high amount of F is suggested for lithofacies afC, indicated by the unique occurrence of deep-violet fluorite in fossil wood, cavities and nodules. Fluorite is recognised as earthy masses and idiomorphic violet cubes, in places with a terminal yellow growth zone. However, an increased F concentration was not evidenced by whole-rock geochemistry (F: 1000 ppm). Nodules of fluorite and hydromuscovite, which are supposed to be of magmatic origin, are found in lithofacies afC and afwbC (F: 1200–2700 ppm). Lithofacies C/euC show distinct geochemical composition regarding a slightly lower Nb/Y ratio (0.23–0.33) and an increased Zr/Ti ratio (0.12–0.14) as a result of low Ti concentrations.

Lithofacies aF and hM show similar geochemical trends in both excavation sites (Fig. 7) in transition to the overlying lithofacies afC/alM (Chemnitz–Hilbersdorf) and aM (Chemnitz–Sonnenberg). Variations in concentrations of SiO_2 and F show a clear opposing trend of both elements, whereas SiO_2 concentration increases upwards in the profile and F concentration decreases. Trends of Zr/Y, Ti/Y and Eu/Eu* trace-element ratios decrease upwards in the profile.

Zircon ages

Analysis-Pb zircon dating via LA ICP-MS is presented in the following and was undertaken to determine the age of eruption for the Zeisigwald tuff and the age of sedimentation for plant fossil bearing strata. The sample from lithofacies afC (Unit S 3) of the Zeisigwald Tuff yielded very few zircons. In total, we mounted and analysed 52 grains and applied 62 U–Pb analyses on them. Fifty-two of all analyses gave a concordant result. Zircon grains vary in size between 40 and 160 µm. They are idiomorphic with clearly evolved surfaces. Some zircons are very long and needle shaped, whereas most are small and compact. They are all prismatic and show sharp edges with nearly no sign of rounding. Most of the analysed zircon grains are colourless, only few are slightly yellow-bright brownish. The CL images of all analysed zircons show diverse internal structures. Most grains exhibit oscillatory magmatic zoning characterised by fine growth zones, but there are also few structures indicating metamorphic overprint (see Fig. 8a). Complex grains show in part xenocrystic cores surrounded by magmatic zoning, e.g., zircon grain with measurements C08 and C09 in Fig. 8c.

The detrital zircon record of the ZTP is dominated by two distinct age peaks (Fig. 9a–c, Table 3: supplementary data). The first one comprises early Permian ages between 290 and 292 Ma. The second one contains Paleozoic to upper Ediacaran ages and ranges from 481 to 675 Ma. These two age peaks summarise more than 92% of all concordant analyses (48/52) and more than 77% of all analyses including also the discordant ones (48/62) for sample VWC 1. The remaining 8% of all concordant analyses are restricted to four analyses with ages > 2 Ga. There is a significant gap of ages between ca. 700 Ma and 2 Ga. The youngest twelve of all concordant analyses resulted in a Concordia age of 291 ± 2 Ma (Fig. 9 d), which is interpreted to be the age of eruption of the Zeisigwald tuff.

The Th/U ratios of all concordant analyses are shown in Fig. 10. The majority of all measurements show values

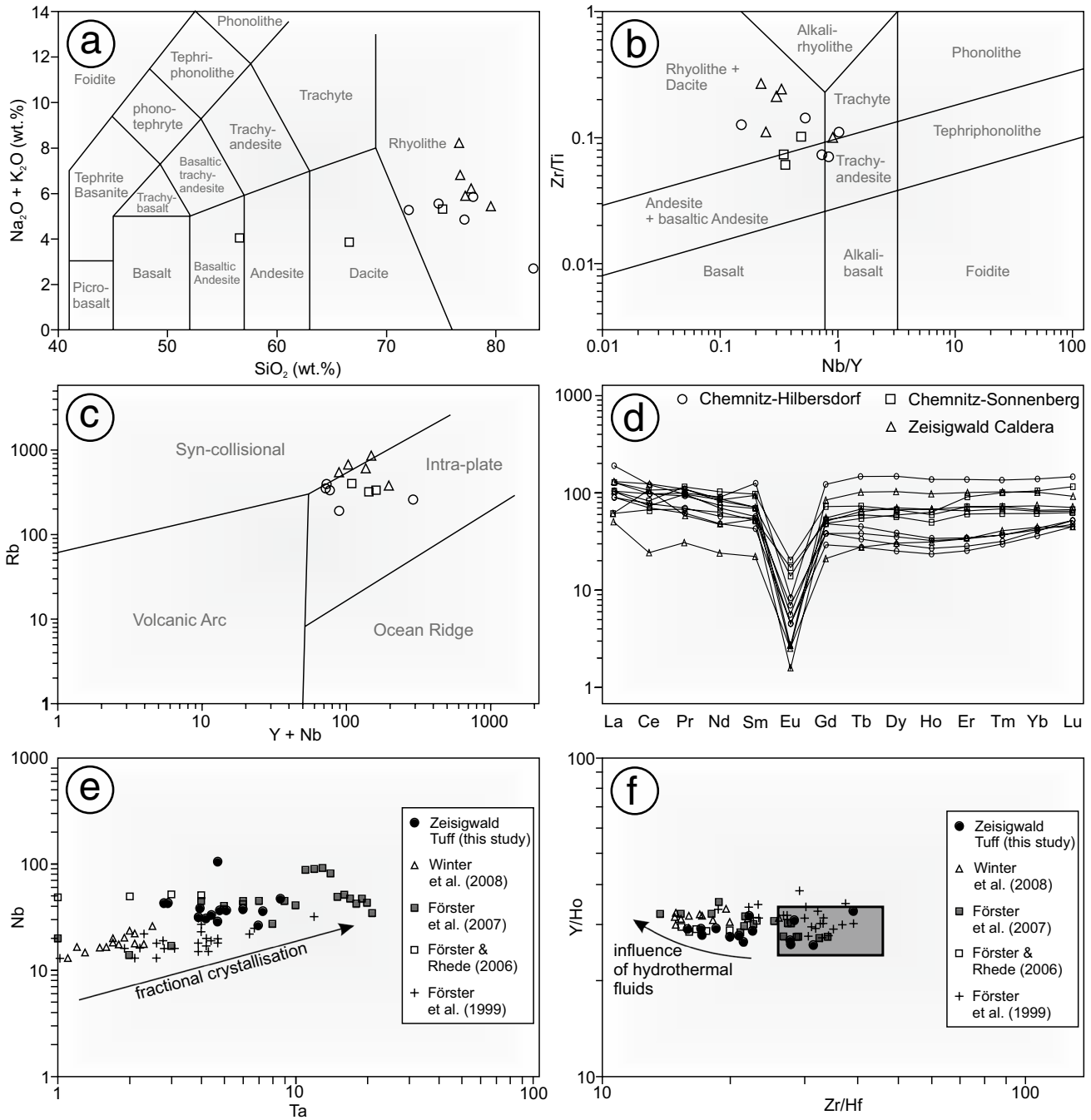

Fig. 6 Whole-rock geochemistry of the ZTP (triangles—Chemnitz–Hilbersdorf excavation, squares—Chemnitz–Sonnenberg excavation, circles—Zeisigwald caldera and others). **a** TAS classification diagram (Le Bas et al. 1986); **b** Classification by immobile trace-element ratios after Pearce (1996), based on Winchester and Floyd (1977); **c** Tectonic discrimination of the Zeisigwald Tuff magma body (Pearce et al. 1984); **d** CI chondrite normalised (after McDonough and Sun 1995) REE concentrations showing distinct "bird-wing" pattern as a result of a significant Eu anomaly and enrichment of HREE; **e** Nb/Ta plot showing degree of fractional crystallisation compared to rhyolitic dikes associated to the Teplice-Altenberg caldera (Winter et al. 2008), rhyolitic dike systems associated to the Erzgebirge granitoids (Förster et al. 2007), Erzgebirge granites of Seiffen (Förster and Rhede 2006), and the other large granitoid intrusions of the Erzgebirge region (Förster et al. 1999); **f** CHARAC diagram ("CHarge And RAdius Controlled" shift of immobile trace-element concentrations after Bau 1996) showing the trace-element shift by the impact of hydrothermal fluida, whereas samples within rectangle show no impact of hydrothermal fluida (for data sources see "e")

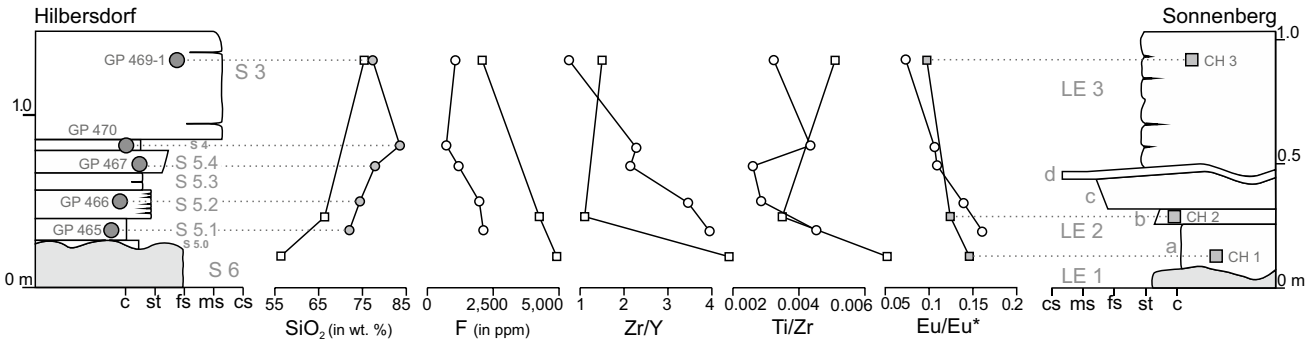

Fig. 7 Trends of selected major and trace elements in the basal pyroclastic succession of the ZTP in the excavation profiles of Chemnitz–Hilbersdorf and Chemnitz–Sonnenberg (grey circles/squares in profiles mark sample origin of whole-rock geochemistry)

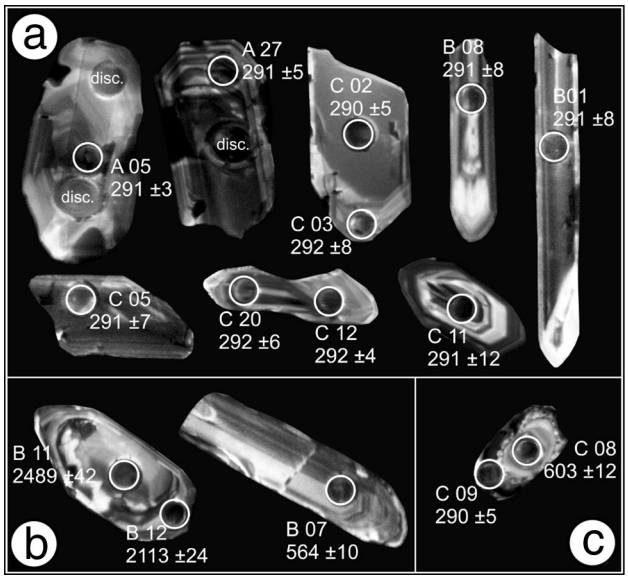

Fig. 8 CL images of representative zircon grains of sample VWC 1. **a** Zircon grains with 9 of the 12 spots used to calculate the extrusion age of 291 ± 2 Ma; **b** Zircon grains showing inherited ages of the Cadomian basement. **c** Zircon grain with core and rim. disc. = discordant analysis. All spots are 25 µm. Given ages refer to the U–Pb age and are in Ma

well below 1.0 and, therefore, plot in the lower part of the diagram representing material derived from felsic melts.

The Hf isotopic results are shown in Fig. 10 b and in Table 4 (supplementary data). The model ages were calculated using a crustal evolution trend of $^{176}Lu/^{177}Hf = 0.0113$. All analysed zircons resulted in distinct negative ε Hf_T values. The ε Hf_T values very between 6 and 10 for the early Permian U–Pb ages and between 3 and 6 for the Paleozoic U–Pb ages. The analysed zircon grain with a Palaeoproterozoic U–Pb age gave an ε Hf_T value of -3.7. The calculated model ages for these negative ε Hf_T values very between 1.3 and 1.5 Ga for the early Permian U–Pb ages and between 1.3 and 1.6 Ga for the Paleozoic U–Pb ages. The 2.05 Ga old zircon core shows a model age of 2.63 Ga. ε Hf values point to a mixing of a younger Variscan and an old Precambrian crust. In the Saxo-thuringian zone the latter one is composed of a mixture of a Cadomian (c. 570–650 Ma) and a ca. 2.0-3.4 Ga old West African cratonic component (Linnemann et al. 2014, 2017). During magma generation for the Zeisigwald eruption, a typical Variscan continental crustal source was reworked. A juvenile component of early Permian magmatic origin was involved only in a low proportion.

Discussion

Interpretation of geochemical data derived from pyroclastic rocks is usually limited by factors such as glass alteration and pyroclastic fractionation (Bachmann et al. 2002). Pyroclastics of the Zeisigwald Tuff succession show permeable fabrics, which are suitable for fluid migration. Consequently, pumice fragments and feldspar crystals are frequently altered to clay minerals. Thus, depletion especially of major elements, such as Ca, Mg, Na and P, but also of some trace elements like Sr and Ba cannot be excluded. Thus, we primarily focus on immobile trace elements to evaluate magmatic processes. Shifts of geochemical composition due to pyroclastic fractionation of mineral aggregates during transport and deposition were only interpreted for lithofacies afC (Unit S3).

Stratigraphic significance

The eruption of the Zeisigwald volcano initiated with a phreatomagmatic explosion of ascending magma coming into contact with groundwater. As a result of the phreatomagmatic influence, a high amount of lithic fragments and inherited zircons was swept along from the metamorphic basement and deposited in these lowermost horizons from which the sample VWC 1 originated (afC; Unit S 3). The inherited zircons frequently consist of an old core and a younger,

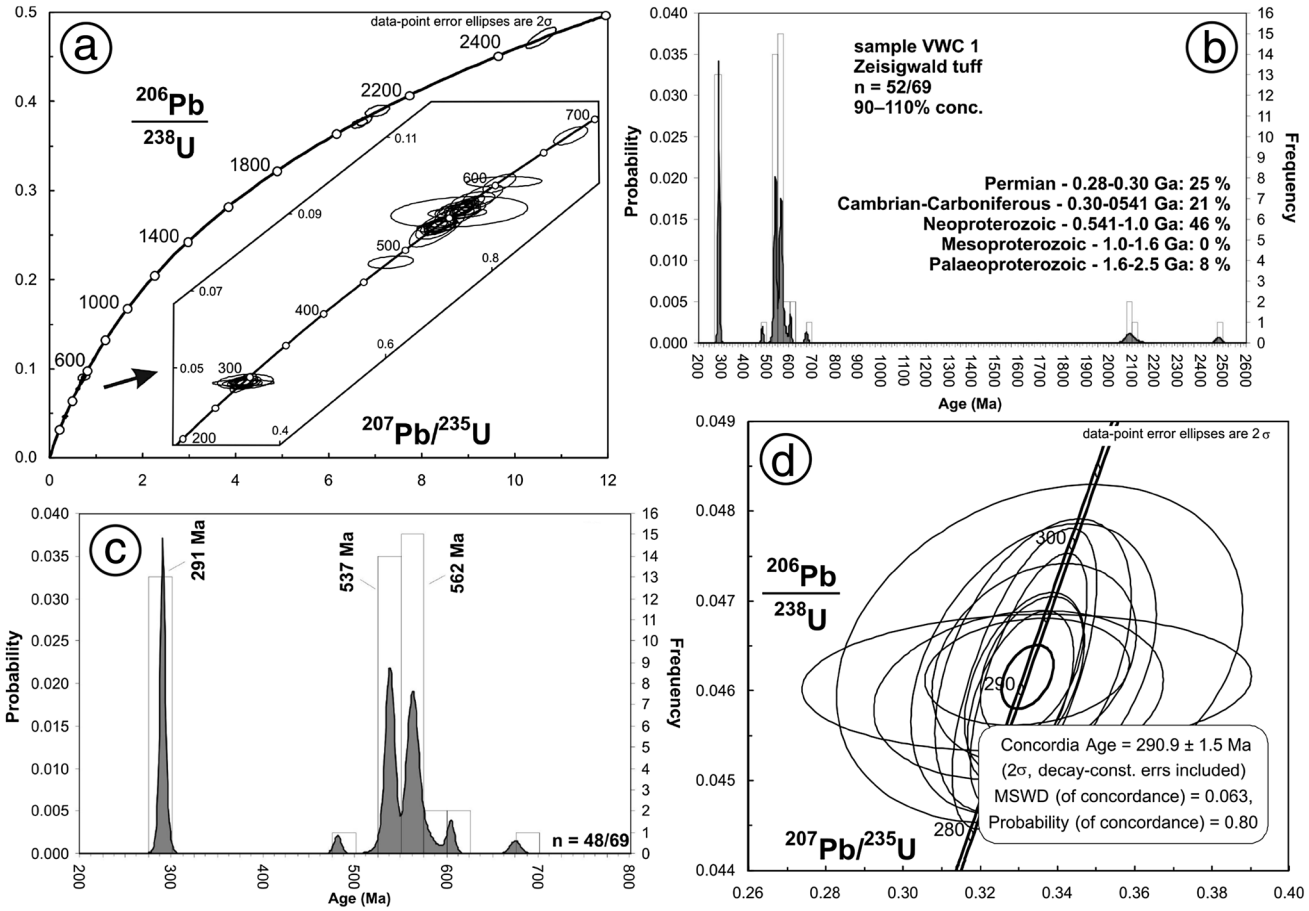

Fig. 9 U–Pb ages of magmatic and inherited zircon grains from sample VWC 1 (afC; unit S 3). **a** Concordia diagram with 2σ error ellipses; **b** combined binned frequency and probability density distribution plots of zircon grains in the range of 200 to 2600 Ma and of, **c** 200 to 800 Ma; **d** concordia plot of U–Pb zircon data of the youngest zircon population of sample VWC 1 with 2σ error ellipses. Concordia age of 291 ± 2 Ma derived from twelve concordant grains, which is interpreted as the age of extrusion

early Permian rim (Fig. 8b, c), exhibiting a nearly perfectly shaped crystal habit. These zircons were assimilated from host rock by the magma of the Zeisigwald volcano during its rise through the crust and acted as crystallisation point for younger rims. Other zircons just show their homogeneous oscillatory zoning without an older core and were thus completely crystallised within the magma chamber. These juvenile crystals show a concordant age of 291 ± 2 Ma (late Sakmarian) that is interpreted as eruption/sedimentation age of the ZTP. All older concordant U–Pb ages are derived from inherited zircons and show Paleozoic, upper Ediacaran and few Palaeoproterozoic ages, and are typically derived from basement rocks of the Saxo-thuringian zone (Linnemann et al. 2014, 2017).

The new age of 291 ± 2 Ma is in good accordance to the previously provided SHRIMP age of 290.6 ± 1.8 Ma (Rößler et al. 2009) and represents a reliable basis for biostratigraphic comparison.

Magma origin and evolution

The evolved felsic magma composition of the ZTP with a high geochemical specialisation was already considered by Rank and Pälchen (1989). In fact, it shows a specialisation similar to late-stage magmatic phases like pegmatitic granitoids. This is indicated by the strongly peraluminous character (Wise and Brown 2010), enrichment in HREE producing bird-wing pattern (Whitworth and Feely 1988) and the relative enrichment of Li, Be, F, Rb, Y, Sn, Cs, Bi, U and Th, compared to the average composition of the upper continental crust (Taylor and McLennan 1985). The distinct Eu anomaly and probably the low Mg and Ca concentrations show that differentiation of plagioclase had been far evolved. In accordance with geochemical data, oscillatory zoning of comparatively narrow and frequent zones observed in the majority of magmatic zircons (Fig. 8a, b), developed during crystallisation from a highly evolved and felsic magma (Corfu et al. 2003).

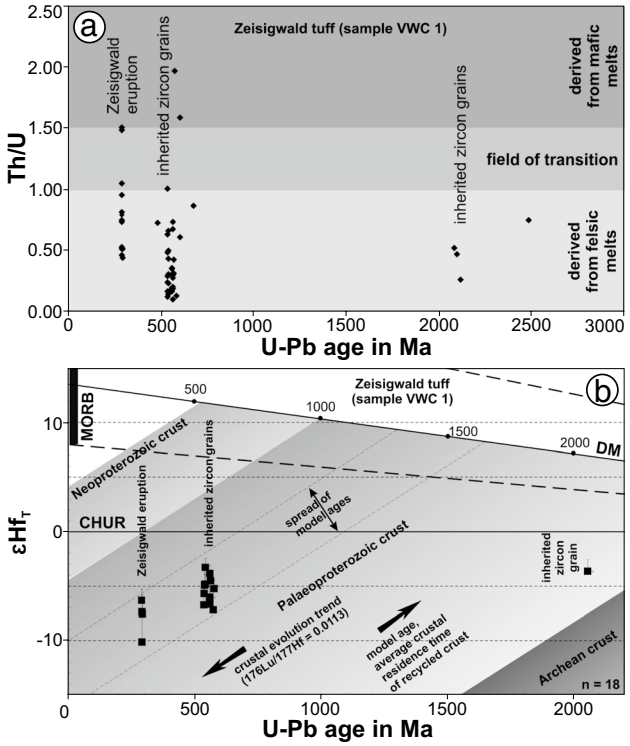

Fig. 10 Interpretation of sample VWC 1 isotopic analysis. **a** Th/U ratios of all analysed zircons concordant in the range of 97 to 100%. Values below 1.0 are typical for a felsic origin of zircon. Ratios significantly above 1.0 point to a mafic origin (Linnemann et al. 2011; Wang et al. 2011); **b** Hf isotope evolution diagram summarizing the data of all zircon grains (see text for discussion). For details and references of depleted mantle evolution see Gerdes and Zeh (2006) and Dhuime et al. (2011). Data were calculated using the decay constant of 1.867×10^{-11} (Scherer et al. 2001) and the CHUR parameters of Bouvier et al. (2008)

The Rb/Y + Nb ratio of the ZTP (Fig. 6c) generally show characteristics typical for the Central Variscides of late-to-post-collisional tectonic regime (Förster et al. 1997, p. 277, Fig. 16). However, high Y concentrations are in better accordance with granites of a post-collisional extensional regime (Fischer 1991; Förster et al. 1997, p. 278, Fig. 17) that was initiated by lower crustal delamination and possibly induced by a mantle-derived heat flow (Pearce et al. 1984). Negative $^{\varepsilon}Hf_T$ isotopic data of sample VWC 1 point to magma that originated from melting of recycled older crust (Fig. 10b). The calculated model ages of inherited zircons, however, spread between 1.3 and 1.6 Ga and are hence not in accordance with the U–Pb ages of the Cadomian crust underlying the Chemnitz Basin. As they are mainly derived from the West African Craton, these units of the Saxo-thuringian zone typically show a gap in U–Pb zircon ages for the Mesoproterozoic (Linnemann et al. 2011, 2014, 2017), which is not the case for the model ages of sample VWC 1. Most probably, the measured $^{\varepsilon}Hf_T$ isotopic values represent mixed values resulting from a mantle input of positive isotopic values and a strong negative input from the old crust. A mixture of both could further explain the "wrong" model ages as they tend to medium values between the young mantle-derived ages and the old crustal-derived ones. This is in agreement with Linnemann et al. (2008, 2014), who gave reason that the Cadomian basement of the Saxo-thuringian zone underwent the same mixing processes. A mantle-derived juvenile input during the Zeisigwald magmatic event is not visible in the $^{\varepsilon}Hf_T$ values, which should show a much wider spread (compare with $^{\varepsilon}$HfT values from Linnemannn et al. 2014). In conclusion, magma of the Zeisigwald volcanism exclusively recycled the local basement of an evolved, crustal source.

Although there is widespread magmatic activity in the Permo-Carboniferous of Saxony (Seckendorff 2012), the co-genetic magmatic relation of the ZTP to spatially associated magmatic complexes has been sparsely discussed, so far (Fig. 1). Both the Schweddey Ignimbrite (Flöha Basin) and the Augustusburg Volcanite are located within a distance of < 8 km from the Zeisigwald eruption centre and show high conformity of geochemical patterns. The Schweddey Ignimbrite has been recently dated by U/Pb measurements to 310 ± 2 Ma (Löcse et al. 2015). Thus, both pyroclastic successions must be regarded as products of temporally isolated volcanic events. However, geochemical similarity of the Schweddey Ignimbrite, the Augustusburg Volcanite and the ZTP suggest a similar magmatic origin. Based on locally high coalification rank of minor Permo-Carboniferous coal seams in the extended study area, a shallow granitic intrusion and/or magmatic hydrothermal activity during the Westphalian was suggested by Weinlich (1983). Deep reaching fault systems, such as the NE–SW trending Central Saxonian Lineament and the NW–SE-trending Flöha Lineament (Schneider et al. 2012) could have favoured ascent of various crustal magma pulses through time resulting in diverse eruptiva.

Relation of the Zeisigwald Volcanic Complex to regional late post-Variscan magmatism has not yet been discussed, although its characteristic high Sn and F concentrations suggest clear similarities to felsic intrusions in the Erzgebirge region (Fig. 1, Seifert and Baumann 1994; Webster et al. 1997), which developed during a time span between 325 and 318 Ma (Förster et al. 1999, 2007; Romer et al. 2007). Similarities become further obvious in $SiO_2/Na_2O + K_2O$ composition, enrichment of mobile trace elements, such as Li, Be, Rb and U, REE patterns as well as Y/Ho and Zr/Hf ratios (Fig. 6 f). Geochemical classification of the Erzgebirge granitoids shows extended compositional heterogeneity (Förster et al. 1999; Fig. 1), whereas A-type granitoid-like high-F and low-P_2O_5 mica granites of Pobershau show good accordance to the ZTP. Among all data, however, the ZTP exhibit the highest geochemical proximity to subvolcanic

rhyolitic dikes spatially associated to the Erzgebirge granitoids (305–295 Ma; Förster et al. 2007). Low CaO_2 and Na_2O concentrations, enriched Li, Be, W,Y trace-elemental composition, the high Nb/Ta ratio implicating far developed fractional crystallisation (Fig. 6e), and extreme REE "bird-wing" pattern (e.g., "Group-III-rhyolite", Förster et al. 2007) suggest a co-genetic relation. In the ZTP, the REE "bird-wing" pattern results from an unusual enrichment of HREE (Fig. 6c), which is referred to high amounts of magmatic garnet (almandine) and phosphate minerals, such as xenotime (YPO_4) in several lithofacies (aF/alM/afC/aM). Low Zr/Hf ratios and slightly higher Y/Ho ratios in the ZTP (Fig. 6f) implicate the lanthanide tetrad effect (enrichment of HREE + Y), which indicates the presence of hydrothermal fluids in highly evolved magmatic systems (Bau 1996; Förster et al. 2007). Due to significant differences of geochemical specialisation, a co-genetic association to the simultaneously occurring and spatially associated volcanism of the North Saxony Volcanic Complex (300 to 290 Ma; Hoffmann et al. 2013), as well as to the much older Teplice-Altenberg Volcanic Complex and associated dike systems (327 to 309 Ma; Winter et al. 2008; Fig. 6e), is rather unlikely.

In conclusion, we propose that magma formation took place in the lower continental crust by re-melting of the old Cadomian basement, initiated by mantle-derived heat flow as a result of crustal delamination (Fig. 11a). The high amount of cadomic zircons in the ZTP was inherited from crustal re-melting and crustal assimilation (Fig. 11b). Magma genesis is probably closely related to granitic intrusions and associated rhyolitic dike systems in the Erzgebirge region (Förster et al. 2007), but also to the nearby Schweddey Ignimbrite and the Augustusburg Volcanite (Löcse et al., under review). During ascend, magma underwent advanced fractional differentiation finally forming a shallow granitic reservoir, from which a smaller chamber of eruptible magma could have developed by crystal–liquid fractionation, which would further explain the exceptionally high evolved and specialised composition of the ZTP (Bachmann and Bergantz 2008, Hildreth and Wilson 2007). Trends of selected immobile trace-element concentrations and ratios in the basal lithofacies aF to afC/aM from base to top could reflect an inverse geochemical zonation in the magma chamber, e.g., decrease of Eu/Eu* ratio by plagioclase fractionation (Fig. 7).

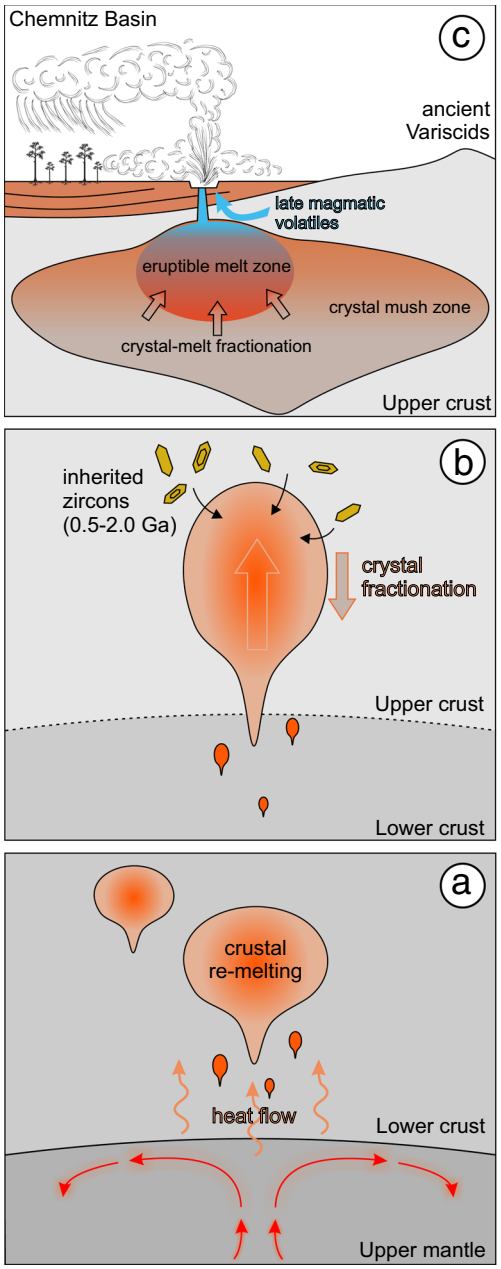

Fig. 11 Magma evolution model of the Zeisigwald Volcanic Complex. **a** Re-melting of lower continental crust of the Cadomic basement induced by a plume-derived mantle heatflow; **b** magma differentiation and uptake of inherited zircons by crustal assimilation during rise of the magma body; **c** Eruption of the shallow magma chamber showing zonation as a result of plagioclase fractionation, and involvement of hydrothermal fluids before and during the eruption

Eruption model and processes

The Zeisigwald eruption is predominantly of phreatomagmatic style and initiated as a result of volatile-rich magma coming in contact with surface-near groundwater. The highly explosive events are characterised by a high degree of fragmentation of pyroclastic material resulting in deposition of predominantly fine to coarse ash tuffs. Deposition of the volcanic succession initiated by low-energy phreatoplinian fallout from a convecting eruption column (aF/hM), whereas inverse gradation indicates vent-widening and increase of eruption energy. Interpreted as a result of eruption column collapse, fallout deposition was continued by local high-aspect ratio, concentrated pyroclastic density

currents (afC/alM, and probably afwbC), which entombed the central part of the Chemnitz Fossil Forest ecosystem (Rößler et al. 2012a). In a second phase, another phreatoplinian eruption with high volatile content and much higher eruption energy produced a mainly air-borne lateral blast causing severe damage to wide areas of the ancient forested landscape quite comparable to the 1980s eruption of Mount St. Helens (Hoblitt et al. 1981; Waitt 1981). In the following, highly fragmented and wet pyroclastic material settled down from the eruption column forming widely distributed, metre-thick fallout deposits, probably with a lateral transport component (aM). The third phase represents the eruption climax and is characterised by major ignimbrite deposits (c/euC) from a rapidly collapsing eruption column with a low volatile content. Eruption is terminated by minor fallout deposits intercalated in the re-sedimentation facies (VC).

Comparable successions are known from several modern and ancient pyroclastic deposits of phreatomagmatic origin (Sparks et al. 1973; Wilson 1985; Allen and Cas 1998). Phreatoplinian eruption style results from volatile-rich magma and/or the presence of surface-near groundwater (Cas and Wright 1987). The transition from wet (aF/alM/afC/aM/afwbC) to dry pyroclastics (C/euC) is thought to reflect deflation of deeper and less volatile-rich magma during the course of eruption. Initially high and later decreasing volatile content is roughly indicated by generally high concentrations of immobile and volatile trace elements, such as F and (H)REE + Y, which slightly decrease in the pyroclastic succession of the ZTP from base to top.

The eruption centre of the Zeisigwald Volcanic Complex is assumed to be located in the Zeisigwald area (Fig. 3), indicated by (1) general decrease of lithofacies thickness from East to West (Fig. 3b), (2) locally welded facies (euC), and (3) local occurrence of lag fall deposits (lB). Thus, pyroclastic deposits generally show a distinct asymmetric distribution, which could be a result of either topography or deposition from an asymmetric bent-over fountain as experimentally shown by Carey et al. (1988). Frequently, deposits resulting from large phreatomagmatic eruptions are accompanied by caldera formation (Heiken and McCoy 1984; Wilson 1985). Eulenberger et. al (1995) interpreted the ring-shaped fault system in the Zeisigwald area (Fig. 3a) as margins of a trapdoor caldera structure, and defined pyroclastics, here indicated as LA 3, as caldera fill deposits, and LA 2 as the corresponding outflow facies (Figs. 2, 3b). In fact, spatial architecture of LA 3 with steep facies gradients could be explained by a morphological depression, probably induced by volcano-tectonic processes. However, lithic breccias as usually strong indicators for caldera structures (Brown et al. 2003), have not been found in the Zeisigwald area. Moreover, mechanism of caldera formation is controlled by deflation rate of the magma chamber and the lithostatic overpressure of the erupted material. Thus, collapse usually occurs during late major ignimbritic eruption phase (Sparks et al. 1973; Self and Rampino 1981). In this context, caldera formation during an early eruption phase (lithofacies aM/afwbC), as suggested by Eulenberger et al. (1995), seems to be unlikely in the Zeisigwald Volcanic Complex, due to the low amount of erupted tephra volume at this time. Therefore, correlation of lithofacies from associations LA 2 and 3 based on compositional and textural characters in drill cores and few outcrops is questionable. Instead, geochemical fingerprint of immobile trace elements in some lithofacies can be used in some cases as a correlation tool, as it was already proposed by Fischer (1991). For example, lithofacies afC (LA 2) and afwbC (LA 3) show clearly enriched Y concentrations compared to the other lithofacies suggesting that both could represent the same depositional unit of the first eruption phase.

In conclusion, the existence of a caldera structure is recently not clearly verifiable for the Zeisigwald Volcanic Complex. Alternatively, a pre-existing depression could have existed, which was filled by early pyroclastics of LA 3. This idea could explain thickness variations already occurring in the basalmost lithofacies of LA 2 and LA 3. Nevertheless, development of a volcano-tectonic sag structure during the ignimbritic eruption phase is not excluded.

Zeisigwald tuff eruption and its taphonomic impact

Interpretation of both sedimentological and geochemical results clearly show that deposition of pyroclastic horizons was a continuous eruption process suggesting a rapid burial of the forest ecosystem and supporting the interpretation of a true T^0 taphocoenosis sensu Gastaldo et al. (1995). Trace-element compositional trends (Fig. 7) seem to represent a valuable proxy to correlate genetically equivalent lithofacies at the two excavation localities of Chemnitz–Hilbersdorf and Chemnitz–Sonnenberg, and potentially elsewhere in the source area.

Magma composition and eruption style have a significant impact on preservation of fossil biota in the Chemnitz Fossil Forest. On the one hand, high volatile content in the magma chamber triggered phreatomagmatic eruption style and deposition of highly fragmented, moist and cool volcanic ashes. On the other hand, the evolved magma was rich in wood petrifaction agents, such as SiO_2 and probably F, favouring a rapid conservation (Rößler and Götze 2000). Fluorite petrifaction of wood is a worldwide matchless phenomenon and interestingly restricted to lithofacies afC (Fig. 5c). Formation process remains still enigmatic, as its origin could be magmatic and/or hydrothermal. Fluorite nodules frequently intergrown with hydromuscovite occurring in lithofacies afwbC are interpreted to be of magmatic origin (Fig. 5c). In addition, cathodoluminescence analysis shows that fluorite formation in the wood occurred during initial petrifaction

(Rößler 2002). Post-depositional hydrothermal formation of fluorite in the highly permeable coarse ash tuff of afC is indicated by fluorite crystals grown in rock cavities.

Conclusion

1. The study represents the first comprehensive synthesis of the Zeisigwald Tuff pyroclastics, combining sedimentological, geochemical and isotopic data to understand in more detail the eruption series responsible for conserving the diverse T^0 taphocoenosis of the Chemnitz Fossil Forest.
2. The new U/Pb radiometric age of 291 ± 2 Ma (LA–ICP–MS) provides a robust late Sakmarian timeline for interregional comparison and correlation of the Chemnitz Fossil Lagerstätte and its striking biota. The age coincides with the previously yielded U/Pb SHRIMP age of 290.6 ± 1.8 Ma (Rößler et al. 2009) and underlines biostratigraphic indications.
3. Zircon U/Pb and Hf isotopes reveal that magma of the Zeisigwald Volcanic Complex recycled lower crust of Cadomian age and assimilated many inherited zircons of Neoproterozoic and Palaeoproterozoic ages. Magma formation was initiated by mantle-derived heat flow probably resulted from a post-orogenetic delamination of continental crust.
4. Highly evolved, felsic composition of the Zeisigwald Tuff pyroclastics points to a high degree of specialisation and incorporation of hydrothermal fluids during ascend. Pyroclastics are hence compositionally akin to nearby Schweddey and Augustusburg volcanites, as well as to Western Erzgebirge granitoids and associated rhyolitic dike intrusions, suggesting a close magma-genetic relation.
5. The Zeisigwald volcanic event is dominated by a series of phreatomagmatic eruptions, which initially deposited wet, cool and highly fragmented ash tuffs, thus favouring the detailed preservation of the ancient forest ecosystem. In the presented facies model, pyroclastic deposits are re-interpreted and formerly proposed caldera formation is challenged.
6. Similar geochemical trends in the basal pyroclastic succession of the Zeisigwald Tuff at Chemnitz–Hilbersdorf and Chemnitz–Sonnenberg reflect reverse differentiation in the magma chamber. The trends indicate a continuous eruption process as well as a simultaneous burial of the forest ecosystem at both localities.

Acknowledgements We highly acknowledge manifold support by our excavation team, especially Ralph Kretzschmar, Volker Annacker, Mathias Merbitz for technical support and Thorid Zierold for dedicated project management. Further we are indebted to Marion Tichomirowa, Christoph Breitkreuz, Alexander Repstock, Klaus-Peter Stanek and Jörg W. Schneider, Freiberg, Sven Eulenberger and Bernd Tunger, Chemnitz and Frank Löcse, St. Egidien for fruitful scientific discussion. We are particularly grateful for financial support by the Deutsche Forschungsgemeinschaft (DFG grant RO 1273/3-1 to RR).

References

Allen SR, Cas RAF (1998) Rhyolitic fallout and pyroclastic density current deposits from a phreatoplinian eruption in the eastern Aegean Sea, Greece. J Volcanol Geotherm Res 86:219–251

Babrauskas V (2001) Ignition of wood: a review of the state of the art. Interflam 2001. Interscience Communications Ltd, London, pp 71–88

Bachmann O, Dungan MA, Lipman PW (2002) The Fish Canyon magma body batholith. J Petrol 43, no.8: pp 1469–1503

Bau M (1996) Controls on the fractionation of isovalent trace elements in magmatic and aqueous systems: evidence from Y/Ho, Zr/Hf, and lanthanide tetrad effect. Contrib Mineral Petrol 123:323–333

Bouvier A, Vervoort JD, Patchet PJ (2008) The Lu-Hf and Sm-Nd isotopic composition of CHUR: constraints from unequilibrated chondrites and implications for the bulk composition of terrestrial planets. Earth Planet Sci Lett 273(1–2):48–57

Breiter K, Novák JK, Chlupáčová M, Republic C (2001) Chemical Evolution of Volcanic Rocks in the Altenberg – Teplice Caldera (Eastern Krušné Hory Mts. Germany) GeoLines 13:17–22

Brown RJ, Barry TL, Branney MJ, Pringle MS, Bryan SE (2003) The Quaternary pyroclastic succession of southeast Tenerife, Canary Islands: explosive eruptions, related caldera subsidence, and sector collapse. Geol Mag 140(3):265–288

Brown RJ, Branney MJ, Maher C, Dávila-Harris P (2009) Origin of accretionary lapilli within ground-hugging density currents: evidence from pyroclastic couplets on Tenerife. GSA Bulletin 122:305–320

Brown RJ, Bonadonna C, Durant AJ (2012) A review of volcanic ash aggregation. Phys Chem Earth 45–46:65–78

Carey SN, Sigurdsson H, Sparks RSJ (1988) Experimental studies of particle-laden plumes. J Geophys Res 93(15):15314–28.

Cas RAF, Wright JV (1987) Volcanic successions—modern and ancient. Chapman and Hall, London, p. 528

Chauvel C, Levin E, Carpentier M, Arndt NT, Marini J-C (2008) Role of recycled oceanic basalt and sediment in generating the Hf-Nd mantle array. Nat Geosci 1:64–67

Cohen KM, Finney SC, Gibbard PL, Fan J-X (2013) updated) The ICS International Chronostratigraphic Chart. Episodes 36:199–204

Corfu F, Hanchar JH, Hoskin PWO, Kinny P (2003) Atlas of Zircon Textures. In: Hanchar JM, Hoskin PWO (eds) Zircon. Reviews in Mineralogy & Geochemistry 53: pp 469–500

Cotta B (1832) Die Dendrolithen in Bezug auf ihren inneren Bau. Arnoldische Buchhandlung, Leipzig und Dresden, p. 89

Dhuime B, Hawkesworth C, Cawood P (2011) When continents formed. Science 331:154–155

DiMichele WA, Falcon-Lang HJ (2011) Pennsylvanian 'fossil forests' in growth position (T0 assemblages): Origin, taphonomic bias and palaeoecological insights. J Geol Soc London 168:585–605

DiMichele WA, Tabor NJ, Chaney DS, Nelson WJ (2006) From wetlands to wet spots: Environmental tracking and the fate of Carboniferous elements in Early Permian tropical floras. In: Greb SF, DiMichele WA (eds) Wetlands through Time. Geol Soc Spec Pap 399: 223–248

Döring H, Fischer F, Rößler R (1999) Sporostratigraphische Korrelation des Rotliegend im Erzgebirge-Becken mit dem Permprofil des Donezk-Beckens. Veröff Mus Naturk Chemnitz 22:29–56

Dunlop JA, Rößler R (2013) The youngest trigonotarbid from the Permian of Chemnitz in Germany. Foss Rec 16(2):229–243
Dunlop JA, Legg DA, Selden PA, Fet V, Schneider JW, Rößler R (2016) Permian scorpions from the Petrified Forest of Chemnitz, Germany. BMC evol biol 16(1):72. https://doi.org/10.1186/s12862-016-0634
Eulenberger S, Tunger B, Fischer F (1995) Neue Erkenntnisse zur Geologie des Zeisigwaldes bei Chemnitz. Veröff Mus Naturk Chemnitz 18:25–34
Eulenberger S, Schneider JW, Rößler R (2010) Die Kernbohrung KB 6 im basalen Zeisigwald-Tuff von Chemnitz-Hilbersdorf. Veröff Mus Naturk Chemnitz 33:113–122
Feng Z, Zierold T, Rößler R (2012) When horsetails became giants. Sci Bull 57:18: 2285–2288
Feng Z, Rößler R, Annacker V, Ji-Yuan Y (2014) Micro-CT investigation of a seed fern (probable medullosan) fertile pinna from the Early Permian Petrified Forest in Chemnitz, Germany. Gondw Res 26:1208–1215
Fischer F (1990) Lithologie und Genese des Zeisigwald-Tuffs (Rotliegendes, Vorerzgebirgs-Senke). Veröff Mus Naturk Chemnitz 14:61–74
Fischer F (1991) Das Rotliegende des ostthüringisch-westsächsischen Raumes (Vorerzgebirgs-Senke, Nordwestsächsischer Vulkanitkomplex, Geraer Becken). Dissertation, Bergakademie Freiberg, unpubl
Fisher RV (1979) Models of pyroclastic surges and pyroclastic flows. J Volcanol Geotherm Res 6:305–318
Förster HJ, Rhede D (2006) The Be–Ta-rich granite of Seiffen (eastern Erzgebirge, Germany): accessory-mineral chemistry, composition, and age of a late-Variscan Li–F granite of A-type affinity. N Jb Miner Abh 182(3):307–321
Förster HJ, Tischendorf G, Trumbull RB (1997) An evaluation of the Rb vs. (Y + Nb) discrimination diagram to infer tectonic setting of silicic igneous rocks. Lithos 40:261–293
Förster HJ, Tischendorf G, Trumbull RB, Gottesmann B (1999) Late-collisional granites in the Variscan Erzgebirge, Germany. J Petrol 40:no 11: 1613–1645
Förster HJ, Gottesmann B, Tischendorf G, Siebel W, Rhede D, Seltmann R, Wasternack J (2007) Permo-Carboniferous subvolcanic rhyolitic dikes in the western Erzgebirge/Vogtland, Germany: a record of source heterogeneity of post-collisional felsic magmatism. N Jb Miner Abh 183(2):123–147
Frei D, Gerdes A (2009) Precise and accurate in situ U-Pb dating of zircon with high sample throughput by automated LA-SF-ICP-MS. Chem Geol 261:261–270
Gastaldo RA, Pfefferkorn HW, DiMichele WA (1995) Characteristics and classification of Carboniferous roof shale floras. Geological Society of America Memoirs 185:341–352
Gerdes A, Zeh A (2006) Combined U-Pb and Hf isotope LA-(MC-) ICP-MS analysis of detrital zircons: comparison with SHRIMP and new constraints for the provenance and age of an Armorican metasediment in Central Germany. Earth Planet Sci Lett 249:47–61
Gerdes A, Zeh A (2009) Zircon formation versus zircon alteration—new insights from combined U-Pb and Lu-Hf in situ LA-ICP-MS analyses, and consequences for the interpretation of Archean zircon from the Central Zone of the Limpopo Belt. Chem Geol 261(3–4):230–243
Green TH (1995) Significance of Nb/Ta as an indicator of geochemical processes in the crust-mantle system. Chem Geol 120:347–359
Heiken G, McCoy F Jr (1984) Caldera development during the Minoan Eruption, Thira, Cyclades, Greece. J Geophys Res 89(B10):8441–8462
Hildreth EW, Wilson CJN (2007) Compositional zoning of the Bishop Tuff. J Petrol 48:951–999
Hilton J, Wang SJ, Galtier J, Glasspool I, Stevens L (2004) An upper Permian permineralized plant assemblage in volcaniclastic tuff from the Xuanwei Formation, Guizhou Province, southern China, and its palaeofloristic significance. Geol Mag 141:661–674
Hoblitt RP, Miller CD, Vallance JW (1981) Origin and stratigraphy of the deposit produced by the May 18 directed blast. US Geol Surv Prof Pap 1250:401–419
Hoffmann U, Breitkreuz C, Breiter K, Sergeev S, Stanek K, Tichomirowa M (2013) Carboniferous–Permian volcanic evolution in Central Europe—U/Pb ages of volcanic rocks in Saxony (Germany) and northern Bohemia (Czech Republic). Int J Earth Sci 102(1):73–99
Kerp H, Noll R, Uhl D (2007) Vegetationsbilder aus dem saarpfälzischen Permokarbon. In: Schindler T, Heidtke UHJ (eds) Kohlesümpfe, Seen und Halbwüsten. Dokumente einer rund 300 Millionen Jahre alten Lebewelt zwischen Saarbrücken und Mainz. Sonderveröffentlichung 10, Pollichia, Bad Dürkheim, pp 76–109
Kretzschmar R, Annacker V, Eulenberger S, Tunger B, Rößler R (2008) Erste wissenschaftliche Grabung im Versteinerten Wald von Chemnitz—ein Zwischenbericht. Freiberger Forschungsheft C 528:25–55
Kroner U, Romer RL (2013) Two plates—many subduction zones: the Variscan orogeny reconsidered. Gondw Res 24:298–329
Le Bas MJ, Le Maitre RW, Streckeisen A, Zanettin B (1986) A chemical classification of volcanic rocks based on the total alkali–silica diagram. J Petrol 27:745–750
Linnemann U, D`Lemos R, Drost K, Jeffries T, Gerdes A, Romer RL, Samson SD, Strachan R (2008) Cadomian tectonics. In: McCann T (ed) The Geology of Central Europe Volume 1: Precambrian and Palaeozoic. Geol Soc London, pp 103–154
Linnemann U, Ouzegane K, Drareni A, Hofmann M, Becker S, Gärtner A, Sagawe A (2011) Sands of West Gondwana: an archive of secular magmatism and plate interactions—a case study from the Cambro-Ordovician section of the Tassili Ouan Ahaggar (Algerian Sahara) using U-Pb LA-ICP-MS detrital zircon ages. Lithos 123:188–203
Linnemann U, Gerdes A, Hofmann M, Marko L (2014) The Cadomian Orogen: neoproterozoic to Early Cambrian crustal growth and orogenic zoning along the periphery of the West African Craton—Constraints from U–Pb zircon ages and Hf isotopes (Schwarzburg Antiform, Germany). Precam Res 244:236–278
Linnemann U, Pidal AP, Hofmann M, Drost D, Quesada C, Gerdes A, Marko L, Gärtner A, Zieger J, Ulrich J, Krause R, Vickers-Rich P, Horak J (2017) A ~ 565 Ma old glaciation in the Ediacaran 1 of peri-Gondwanan West Africa. Int J Earth Sci. https://doi.org/10.1007/s00531-017-1520-7
Löcse F, Linnemann U, Schneider G, Annacker V, Zierold T, Rößler R (2015) 200 Jahre Tubicaulis solenites (Sprengel) Cotta. Sammlungsgeschichte, Paläobotanik & Geologie eines oberkarbonischen Baumfarn-Unikats aus dem Schweddey-Ignimbrit vom Gückelsberg bei Flöha. Veröff Mus Naturk Chemnitz 38:5–46
Löcse F, Linnemann U, Schneider G, Merbitz M, Rößler R (under review) First U-Pb LA-ICP-MS zircon ages and zircon morphology investigations assessed from a volcano-sedimentary complex of the mid-European Variscids (Pennsylvanian, Flöha Basin, SE Germany). Int J Earth Sci
Ludwig KR (2001) Users manual for Isoplot/Ex rev. 2.49. berkeley geochronology center special publication 1a: pp 1–56
Luthardt L, Rößler R (2017) Fossil forest reveals sunspot activity in the early Permian. Geology 45(3):279–282. https://doi.org/10.1130/G38669.1
Luthardt L, Rößler R, Schneider JW (2016) Palaeoclimatic and site-specific conditions in the early Permian fossil forest of

Chemnitz—sedimentological, geochemical and palaeobotanical evidence. Palaeogeogr Palaeoclimatol Palaeoecol 441:627–652. https://doi.org/10.1016/j.palaeo.2015.10.015

Luthardt L, Rößler R, Schneider JW (2017) Tree-ring analysis appraising the fourth dimension of an in situ fossil forest and elucidating the last 80 years of an early Permian ecosystem. Palaeogeogr Palaeoclimatol Palaeoecol 487:278–295. https://doi.org/10.1016/j.palaeo.2017.09.011

Major JJ, Pierson TC, Hoblitt RP, Moreno H (2013) Pyroclastic density currents associated with the 2008–2009 eruption of Chaitén Volcano (Chile): forest disturbances, deposits, and dynamics. And Geol 40(2):324–358. https://doi.org/10.5027/andgeoV40n2-a09

Mason BG, Pyle DM, Oppenheimer C (2004) The size and frequency of the largest explosive eruptions on Earth. Bull Volcanol 66:735–748. https://doi.org/10.1007/s00445-004-0355-9

McDonough WF, Sun SS (1995) The composition of the Earth. Chem Geol 120:223–253

Mißbach K (1973) Waldbrand—Verhütung und Bekämpfung. VEB Deutscher Landwirtschaftsverlag, Berlin, pp 16–23

Nasdala L, Götze J, Pidgeon RT, Kempe U, Seifert T (1998) Constraining a SHRIMP U-Pb age: micro-scale characterization of zircons from Saxonian Rotliegend rhyolites. Contrib Mineral Petrol 132:300–306

Newhall CG, Self S (1982) The volcanic explosivity index (VEI): an estimate of explosive magnitude for historical volcanism. J Geophys Res 87:1231–1238

Opluštil S, Pšenička J, Bek J, Wang J, Feng Z, Libertin M, Šimůnek Z, Bureš J, Drábková J (2014) T^0 peat-forming plant assemblage preserved in growth position by volcanic ash-fall: a case study from the Middle Pennsylvanian of the Czech Republic. Bull Geosci 89(4):773–818

Pearce JA (1996) A User's Guide to Basalt Discrimination Diagrams. In: Wyman DA (ed). Trace element geochemistry of volcanic rocks: applications for massive sulphide exploration. Geological Association of Canada, Short Course Notes 12, pp. 79–113

Pearce JA, Harris NBW, Tindle AG (1984) Trace element discrimination diagrams for the tectonic interpretation of granitic rocks. J Petrol 25:956–983

Rank G, Pälchen W (1989) Zur Geochemie der sauren postvariszischen Vulkanite im Raum Flöha—Karl-Marx-Stadt. Z geol Wiss Berlin 17:1087–1097

Repstock A, Breitkreuz C, Lapp M, Schulz B (2017) Voluminous and crystal-rich igneous rocks of the Permian Wurzen volcanic system, northern Saxony, Germany: physical volcanology and geochemical characterization. Int J Earth Sci. https://doi.org/10.1007/s00531-017-1554-x

Romer RL, Thomas R, Stein HJ, Rhede D (2007) Dating multiply overprinted Sn-mineralized granites—examples from the Erzgebirge. Germany Miner Deposita 42:337–359

Roscher M, Schneider JW (2006) Permo-Carboniferous climate: Early Pennsylvanian to late Permian climate development of central Europe in a regional and global context. In: Lucas SG, Cassinis G, Schneider JW (eds) Non-marine permian biostratigraphy and biochronology. Geol Soc Lon Spec Publ 265: 95–136

Rößler R (ed) (2001) Der Versteinerte Wald von Chemnitz. Katalog zur Ausstellung Sterzeleanum. 253 pp., Chemnitz (Museum für Naturkunde)

Rößler R (2002) Study methods for determining the structure of plant organs. In: Dernbach U, Tidwell WD (eds) Geheimnisse versteinerter Pflanzen. D'Oro, Heppenheim

Rößler R, Götze J (2000) Kathodolumineszenz-Untersuchungen an Kieselhölzern—I. Silifizierungen aus dem Versteinerten Wald von Chemnitz (Perm, Deutschland). Veröff Mus Naturk Chemnitz 23:35–50

Rößler R, Annacker V, Kretzschmar R, Eulenberger S, Tunger B (2008) Auf Schatzsuche in Chemnitz—Wissenschaftliche Grabungen '08. Veröff Mus Naturk Chemnitz 31:5–44

Rößler R, Kretzschmar R, Annacker V, Mehlhorn S (2009) Auf Schatzsuche in Chemnitz – Wissenschaftliche Grabungen `09. Veröff Mus Naturk Chemnitz 32:25–46

Rößler R, Kretzschmar R, Annacker V, Mehlhorn S, Merbitz M, Schneider JW, Luthardt L (2010) Auf Schatzsuche in Chemnitz—Wissenschaftliche Grabungen '10. Veröff Mus Naturk Chemnitz 33:27–50

Rößler R, Zierold T, Feng Z, Kretzschmar R, Merbitz M, Annacker V, Schneider JW (2012a) A snapshot of an Early Permian ecosystem preserved by explosive volcanism: new results from the petrified forest of Chemnitz. Germany Palaois 27:814–834

Rößler R, Feng Z, Noll R (2012b) The largest calamite and its growth architecture—arthropitys bistriata from the Permian petrified forest of Chemnitz. Rev Palaeobot Palynol 185:64–78

Rößler R, Merbitz M, Annacker V, Luthardt L, Noll R, Neregato R, Rohn R (2014) The root systems of Permian arborescent sphenopsids: evidence from the Northern and Southern hemispheres. Palaeontographica B 291(4–6):65–107

Rowley PD, Kuntz MA, Macleod NS (1981) Pyroclastic Flow Deposits. In: Lipman PW, Mullineaux DR (eds) The 1980 eruptions of Mount St. Helens, Washington. USGS Professional Paper 1250: 489–512, Washington, D.C.

San Juan Volcanic Field, Colorado: rejuvenation and eruption of an upper-crustal

Scherer E, Münker C, Mezger K (2001) Calibration of the Lutetium-Hafnium clock. Science 293:683–687

Schmincke H-U, Fisher RV, Waters AC (1973) Antidune and chute and pool structures in base surge deposits of the Laacher See area, Germany. Sedimentology 20:553–574

Schneider JW (1994) Environment, biotas and taphonomy of the Lower Permian lacustrine Niederhäslich limestone, Döhlen basin, Germany. Trans R Soc Edinburgh 84:453–464

Schneider JW, Scholze F (2016) Late Pennsylvanian—early triassic conchostracan biostratigraphy: a preliminary approach. In: Lucas SG, Shen SZ (eds) The permian timescale. Geol Soc Lon Spec Publ 450, London

Schneider JW, Werneburg R (2012) Biostratigraphie des Rotliegend mit Insekten und Amphibien. In: Dt Strat Komm (ed) Stratigraphie von Deutschland X. Rotliegend. Teil I: Innervariscische Becken. Schriftenreihe Dt Ges Geowiss 61, Hannover, 110–142

Schneider JW, Rößler R, Fischer F (2012) Rotliegend des Chemnitz-Beckens. In: Dt Strat, Komm (eds) Stratigraphie von Deutschland X. Rotliegend. Teil I: Innervariscische Becken. Schriftenreihe Dt Ges Geowiss 61, Hannover, 530–588

Schumacher R, Schmincke H-U (1991) Internal structure and occurrence of accretionary lapilli: a case study at Laacher See volcano. Bull Volcanol 53:612–634

Scott AC, Brown R, Galtier J, Meyer-Berthaud B (1994) Fossil plants from the Viséan of East Kirkton, West Lothian, Scotland. Trans R Soc Edinburgh 84:249–260

Seckendorff V von (2012) Der Magmatismus in und zwischen den spätvariscischen permokarbonen Sedimentbecken in Deutschland. In: Dt Strat, Komm (eds) Stratigraphie von Deutschland X. Rotliegend. Teil I: Innervariscische Becken. Schriftenreihe Dt Ges Geowiss 61, Hannover, 743–860

Seifert T, Baumann L (1994) On the metallogeny of the Central Erzgebirge Anticlinal Area (Marienber District), Saxony, Germany. Monograph Series of Mineral Deposits 31:169–190

Self S (1983) Large-scale phreatomagmatic silicic volcanism: a case study from New Zealand. In: Sheridan MF, Barberi F (eds) Explosive Volcanism. J Volcanol Geotherm Res 17: 433–469

Self S, Rampino MR (1981) The 1883 eruption of Krakatau. Nature 294:699–704

Self S, Sparks RSJ (1978) Characteristics of widespread pyroclastic deposits formed by the interaction of silicic magma and water. Bull Volcanol 41(3):196–212

Sircombe KN (2004) AGE DISPLAY: an EXCEL workbook to evaluate and display univariate geochronological data using binned frequency histograms and probability density distributions. Comput Geosci 30:21–31

Sláma J, Košler J, Condon DJ, Crowley JL, Gerdes A, Hanchar JM, Horstwood MSA, Morris GA, Nasdala L, Norberg N, Schaltegger U, Schoene B, Tubret MN, Whitehouse MJ (2008) Plešovice zircon—a new natural reference material for U-Pb and Hf isotopic microanalysis. Chem Geol 249:1–35

Sohn YK, Chough SK (1989) Depositional processes of the Suwolbong tuff ring, Cheju Island (Korea). Sedimentology 36:837–855

Sparks RSJ, Self S, Walker GPL (1973) Products of ignimbrite eruptions. Geology 4:115–118

Spicer RA (1989) The formation and interpretation of plant fossil assemblages. Adv Bot Res 16:95–191

Spindler F, Werneburg R, Schneider JW, Luthardt L, Annacker V, Rößler R (2018) First arboreal 'pelycosaurs' (Synapsida: Varanopidae) from the early Permian Chemnitz Fossil Lagerstätte, SE-Germany. Pal Z (**in press**)

Stacey JS, Kramers JD (1975) Approximation of terrestrial lead isotope evolution by a two-stage model. Earth Planet Sci Lett 26:207–221

Sulpizio R, Mele D, Dellino P, la Volpe L (2007) Deposits and physical properties of pyroclastic density currents during complex Subplinian eruptions: the AD 472 (Pollena) eruption of Somma-Vesuvius, Italy. Sedimentology 54:607–635

Swanson FJ, Jones JA, Crisafulli CM, Lara A (2013) Effects of volcanic and hydrologic processes on forest vegetation: Chaitén Volcano, Chile. And Geol 40(2):359–391

Taylor SR, McLennan SM (1985) The continental crust: its composition and evolution. Blackwell, Oxford, p 312

Tunger B, Eulenberger S (2001) Der Hornstein von Chemnitz-Altendorf im Aufschluss—Lithofazielle Beobachtungen und ihre Interpretation. Veröff Mus Naturk Chemnitz 24:23–30

Waitt RB (1981) Devastating pyroclastic density flow and attendant air fall of May 18 – stratigraphy and sedimentology of deposits. In: Lipman PW, Mullineaux DR (eds) The 1980 Eruptions of Mount St. Helens, Washington. US Geol Surv Prof Pap 1250: 439–460

Walker GPL, Heming RF, Sprod TJ, Walker HR (1981) Last major eruptions of Rabaul volcano. Geol Surv Papua New Guinea Mem 10:181–194

Wang X, Griffin WL, Chen J, Huang P, Li X (2011) U and Th contents and Th/U ratios of zircon in felsic and mafic magmatic rocks: improved zircon-melt distribution coefficients. Acta Geol Sin 85(1):164–174

Wang J, Pfefferkorn HW, Zhang YI, Feng Z (2012) Permian vegetational Pompeii from Inner Mongolia and its implications for landscape paleoecology and paleobiogeography of Cathaysia. PNAS 109(13):4927–4932

Webster JD, Thomas R, Rhede D, Förster HJ, Seltmann R (1997) Melt inclusions in quartz from an evolved peraluminous pegmatite: geochemical evidence for strong tin enrichment in fluorine-rich and phosphorous-rich residual liquids. Geochim Cosmochim Acta 61(13):2589–2604

Weinlich FH (1983) Zur Inkohlungsproblematik der Kohlen des Gebietes Karl-Marx-Stadt—Flöha. Zeitschrift für angewandte Geologie 29(8):385–390

Whalen JB, Currie KL, Chappell BW (1987) A-type granites: geochemical characteristics, discrimination and petrogenesis. Contrib Mineral Petrol 95:407–419

Whitworth MP, Feely M (1988) The geochemistry of selected pegmatites and their host granites from the Galway Granite, western Ireland. Irish J Earth Sci 10(1):89–97

Wilson CJN (1985) The Taupo eruption, New Zealand I. General aspects. Phil Trans R Soc Lond A 314:229–310

Wilson L, Sparks RSJ, Walker GPL (1980) Explosive volcanic eruptions—IV. The control of magma properties and conduit geometry on eruption column behaviour. Geophys J R Astr Soc 63:117–148

Winchester JA, Floyd PA (1977) Geochemical discrimination of different magma series and their differentiation products using immobile elements. Chem Geol 20:325–343

Winter C, Breitkreuz C, Lapp M (2008) Textural analysis of a Late Palaeozoic coherent-pyroclastic rhyolitic dyke system near Burkersdorf (Erzgebirge, Saxony, Germany). Geol Soc Lon Spec Publ 302:199–221

Wise MA, Brown CD (2010) Mineral chemistry, petrology and geochemistry of the Sebago granite–pegmatite system, southern Maine, USA. J Geosc 55:3–26. https://doi.org/10.3190/jgeosci.061

Wohletz KH, Sheridan MF (1979) A model of pyroclastic surge. GSA Special Papers 180:177–194

Wohletz KH, McGetchin TR, Sandford MT, Jones EM (1984) Hydrodynamic aspects of caldera-forming eruptions: numerical models. J Geophys Res 89:8269–8285

Wright JV, Walker GPL (1977) The ignimbrite source problem: significance of co-ignimbrite lag-fall deposit. Geology 5:729–732